

RESEARCH ARTICLE

10.1002/2017JA024555

Special Section:

Magnetospheric Multiscale (MMS) Mission Results Throughout the First Primary Mission Phase

Key Points:

- We motivate a theory of the guide field dependence of the location within the diffusion region of X line, stagnation points, and nonzero $\mathbf{J} \cdot \mathbf{E}'$
- Two-dimensional PIC simulations of three MMS events confirm location of energy conversion moves toward electron stagnation point with increasing guide field
- Reconnection rate in 2-D PIC simulations agrees well with AMPERE observations and global simulations but are far lower than MMS observations

Supporting Information:

- Movie S1
- Movie S2
- Movie S3

Correspondence to:

P. A. Cassak,
Paul.Cassak@mail.wvu.edu

Citation:

Cassak, P. A., Genestreti, K. J., Burch, J. L., Phan, T.-D., Shay, M. A., Swisdak, M., ... Komar, C. M. (2017). The effect of a guide field on local energy conversion during asymmetric magnetic reconnection: Particle-in-cell simulations. *Journal of Geophysical Research: Space Physics*, 122, 11,523–11,542. <https://doi.org/10.1002/2017JA024555>

Received 9 JUL 2017













Accepted 17 OCT 2017

Accepted article online 31 OCT 2017

Published online 30 NOV 2017

©2017. American Geophysical Union.
All Rights Reserved.

The Effect of a Guide Field on Local Energy Conversion During Asymmetric Magnetic Reconnection: Particle-in-Cell Simulations

P. A. Cassak¹ , K. J. Genestreti², J. L. Burch³ , T.-D. Phan⁴ , M. A. Shay⁵ , M. Swisdak⁶ , J. F. Drake⁶ , L. Price⁶ , S. Eriksson⁷ , R. E. Ergun^{7,8} , B. J. Anderson⁹ , V. G. Merkin⁹ , and C. M. Komar^{10,11} 

¹Department of Physics and Astronomy, West Virginia University, Morgantown, WV, USA, ²Space Research Institute, Austrian Academy of Sciences, Graz, Austria, ³Southwest Research Institute, San Antonio, TX, USA, ⁴Space Sciences Laboratory, University of California, Berkeley, CA, USA, ⁵Bartol Research Institute, Department of Physics and Astronomy, University of Delaware, Newark, DE, USA, ⁶IREAP, University of Maryland, College Park, MD, USA, ⁷Laboratory for Atmospheric and Space Physics, University of Colorado Boulder, Boulder, CO, USA, ⁸Department of Astrophysical and Planetary Sciences, University of Colorado Boulder, Boulder, CO, USA, ⁹The Johns Hopkins University Applied Physics Laboratory, Laurel, MD, USA, ¹⁰Geospace Physics Laboratory, NASA Goddard Space Flight Center, Greenbelt, MD, USA, ¹¹Department of Physics, Catholic University of America, Washington, DC, USA

Abstract We use theory and simulations to study how the out-of-plane (guide) magnetic field strength modifies the location where the energy conversion rate between the electric field and the plasma is appreciable during asymmetric magnetic reconnection, motivated by observations (Genestreti et al., 2017). For weak guide fields, energy conversion is maximum on the magnetospheric side of the X line, midway between the X line and electron stagnation point. As the guide field increases, the electron stagnation point gets closer to the X line, and energy conversion occurs closer to the electron stagnation point. We motivate one possible nonrigorous approach to extend the theory of the stagnation point location to include a guide field. The predictions are compared to two-dimensional particle-in-cell (PIC) simulations with vastly different guide fields. The simulations have upstream parameters corresponding to three events observed with Magnetospheric Multiscale (MMS). The predictions agree reasonably well with the simulation results, capturing trends with the guide field. The theory correctly predicts that the X line and stagnation points approach each other as the guide field increases. The results are compared to MMS observations, Active Magnetosphere and Planetary Electrodynamics Response Experiment (AMPERE) observations of each event, and a global resistive-magnetohydrodynamics simulation of the 16 October 2015 event. The PIC simulation results agree well with the global observations and simulation but differ in the strong electric fields and energy conversion rates found in MMS observations. The observational, theoretical, and numerical results suggest that the strong electric fields observed by MMS do not represent a steady global reconnection rate.

1. Introduction

Magnetic reconnection is an important aspect of dynamics in planetary magnetospheres, the solar corona, magnetically confined fusion devices, and astrophysical settings (e.g., Zweibel & Yamada, 2009). In Earth's magnetosphere, it is a crucial part of the global convection process (Dungey, 1953, 1961) and the abrupt release of magnetic energy in the magnetotail during storms and substorms (Angelopoulos et al., 2013; McPherron et al., 1973). One of the key questions about reconnection is the nature of the conversion of magnetic energy to plasma energy during the process. This happens both at the microscopic scale, immediately near the diffusion region where magnetic topology changes (e.g., Pritchett, 2006) or at current filaments where reconnecting sheets become turbulent (Fu et al., 2017) and at the macroscopic/mesosopic scale as reconnected magnetic field lines retract and accelerate and heat the plasma in the exhaust (e.g., Drake et al., 2006). The energy conversion contains both reversible and irreversible parts; irreversible dissipation occurs both where counterstreaming beams in reconnection exhausts thermalize (Egedal et al., 2015; Haggerty et al., 2015) and are a crucial necessity where the frozen-in condition breaks down in the diffusion region. The latter was a strong motivation for the Magnetospheric Multiscale (MMS) mission (Burch, Moore, et al., 2016), which was designed to resolve physics at and below electron scales.

The present study is motivated by recent results from the MMS mission. The first dayside magnetopause phase (1a) resulted in 12 crossings that were electron diffusion region candidates. These events had a significant spread in the local parameters thought to control the local reconnection process (Fuselier et al., 2017). We do not attempt to review the large body of work on all of these events. Instead, we focus on three particular events: 16 October 2015 (Burch, Torbert, et al., 2016), 8 December 2015 (Burch & Phan, 2016), and 8 September 2015 (Eriksson, Lavraud, et al., 2016; Eriksson, Wilder, et al., 2016). An interesting observation was made in a companion study (Genestreti et al., 2017) about the location where the rate at which work is done by the electric field \mathbf{E} in the reference frame of the electrons $\mathbf{J} \cdot \mathbf{E}'$, where \mathbf{J} is the current density and the prime on \mathbf{E} denotes that it is evaluated in the local reference frame where the perpendicular electron bulk flow velocity is zero (Zenitani et al., 2011). The strongest signal of $\mathbf{J} \cdot \mathbf{E}'$ was on the magnetospheric side of the magnetic field reversal in the 16 October 2015 event, and that event had a weak out-of-plane (guide) magnetic field of strength about 0.1 of the reconnecting magnetic field in the magnetosheath. In the 8 December 2015 event, there was structure in $\mathbf{J} \cdot \mathbf{E}'$ in two places—near the field reversal and on the magnetospheric side of it, and the guide field was about the same strength as the magnetosheath reconnecting field. In the 8 September 2015 event, the $\mathbf{J} \cdot \mathbf{E}'$ signal was strong very close to the field reversal, and the guide field was about 5 times the reconnection sheath field strength. On the basis of these results, it was suggested that the strength of the guide field is a crucial determining factor of the location within the diffusion region where the rate of work done by the electric field is significant (Genestreti et al., 2017).

The purpose of the present study is to address this question theoretically and numerically. On the theoretical side, the challenge is that dayside reconnection is typically asymmetric (Levy et al., 1964), meaning that the magnetic fields, densities, and temperatures on the two upstream sides of the reconnection region are unequal. Of course, the location of maximum work done by the electric field in symmetric reconnection is at the symmetry point—the X line where the field topology changes, which is coincident with the stagnation point where the in-plane flow goes to zero. In asymmetric reconnection, the diffusion region develops a more complicated substructure where the X line and stagnation point are not colocated (Cassak & Shay, 2007). In the collisionless reconnection regime as is appropriate for Earth's magnetosphere, it is even more complicated because electrons and ions have separate stagnation points (Cassak & Shay, 2009). Understanding where energy conversion occurs requires an understanding of the diffusion region substructure, but this has not been addressed for systems with a guide field. These questions are relevant to other settings where asymmetric reconnection occurs, including Earth's magnetotail (Hietala et al., 2017; Øieroset et al., 2004), laboratory experiments (Yoo et al., 2014), turbulence (Servidio et al., 2009, 2010), solar physics (Murphy et al., 2012), and at other planetary magnetospheres (DiBraccio et al., 2013; Fuselier et al., 2014; Masters et al., 2012).

In this study, we qualitatively motivate how a guide field changes the location where $\mathbf{J} \cdot \mathbf{E}'$ stop is nonzero, arguing that it is midway between the X line and electron stagnation point for weak guide fields and moves toward the electron stagnation point with increasing guide field (for typical magnetospheric conditions). Then, we discuss the quantitative dependence on guide field of the diffusion region substructure, i.e., the location of the X line and stagnation points. The goal here is to gain the ability to make approximate quantitative predictions of the substructure of the diffusion region and therefore the region where $\mathbf{J} \cdot \mathbf{E}'$ is nonzero.

The predictions are compared with particle-in-cell (PIC) simulations. Rather than a simulation study which is organized to have the guide field systematically varied, we opt to perform two-dimensional (2-D) simulations with upstream parameters meant to represent the parameters observed in the three MMS reconnection events motivating this study. This approach makes it more challenging to definitively attribute effects to the strength of the guide field, but has the advantage of allowing us to compare the simulation results more directly to the observations of the events in question. We focus only on the three events discussed here because of their range in guide field; we leave other events and parameter ranges for future work. As signatures of the process, we investigate the simulated reconnection rates, the rate of work done by the electric field, and the distribution functions of electrons within the diffusion region that reveal the mechanism for the generation of current. We find the theoretical arguments, while not perfect, do help organize the data and provide perspective on the location where $\mathbf{J} \cdot \mathbf{E}'$ is.

The PIC simulation results are then compared to observations, where similarities and differences are noted. We conclude, as has been anticipated (Ergun et al., 2016; Eriksson, Wilder, et al., 2016), that the strongest electric field signals and rate of work done by the electric field in the MMS data far exceed those seen in the 2-D simulations and predicted by theory. However, we also compare the results with local and global measures of the

reconnection rate inferred from observations from the Active Magnetosphere and Planetary Electrodynamics Response Experiment (AMPERE) and global magnetospheric resistive-magnetohydrodynamics (MHD) simulations. We find that the agreement with these global and local reconnection rates are quite reasonable. These results collectively suggest that the strong electric field signals observed with MMS for these three events are not the large-scale reconnection electric fields of 2-D steady state reconnection and therefore represent something different. This could include 3-D effects, time dependence of the reconnection process, an inherent spatial burstiness of the reconnection process, external effects that impact reconnection on the microscopic scales, or that the measured electric fields represent some other effect.

The layout of this manuscript is as follows. Theoretical motivation of the location where $\mathbf{J} \cdot \mathbf{E}'$ is nonzero and the relative and absolute locations of the X line and stagnation points are given in section 2. The simulations and how they are set up are described in section 3. Section 4 gives the results of the simulations. Section 5 discusses the results in context of the MMS observations of the three events in question, and discusses comparisons with AMPERE observations and global MHD simulations. Finally, section 6 provides further discussion and conclusions.

2. Theory

In asymmetric reconnection, the peak in $\mathbf{J} \cdot \mathbf{E}'$ need not be at the X line and, indeed, is typically not. For this discussion, we use boundary normal coordinates where L is the direction of the reconnecting magnetospheric magnetic field corresponding to the outflow direction, N is the outward magnetospheric normal direction corresponding to the inflow direction, and $\hat{\mathbf{M}} = \hat{\mathbf{N}} \times \hat{\mathbf{L}}$ completes the triplet and is out of the reconnection plane. We seek the location in the inflow N direction where $\mathbf{J} \cdot \mathbf{E}'$ is nonzero for asymmetric reconnection and its dependence on guide field. We treat only 2-D reconnection in the steady state. We define the X line location in N as X , and the electron and ion stagnation points as S_e and S_i , respectively.

Contributions to $\mathbf{J} \cdot \mathbf{E}'$ can be broken down into two parts. One is due to current out of the reconnection plane $J_M E'_M$, that is, parallel to the X line. This is expected to be the most significant contribution for reconnection with an appreciable guide field, as particles accelerate along the magnetic field due to the out-of-plane (reconnection) electric field E'_M . The other part, $\mathbf{J}_\perp \cdot \mathbf{E}'_\perp$, comes from motion in the reconnection plane, perpendicular (\perp) to the X line. We expect this to be the most important contribution in the weak guide field limit, as explained below.

We first consider the weak guide field case. In 2-D asymmetric reconnection with parameters typical of Earth's dayside magnetopause, the normal (Hall) electric field E_N points from the magnetospheric side toward the magnetosheath and is predominantly on the magnetospheric side of the X line (see, e.g., Figure 1 in Shay et al., 2016). The magnetosheath electrons cross the X line toward the magnetospheric side (Cassak & Shay, 2008). This produces a magnetosheath-directed J_N , so $J_N E_N$ is positive because the normal electric field does work on electrons when they are accelerated by the Hall electric field. Since the bulk electron flow goes to zero at the electron stagnation point, $J_N E_N$ is relatively small there. Since the electrons accelerated by the Hall electric field have already crossed the X line, the location where $J_N E_N$ is maximum for the weak guide field case is expected to be between the X line and the electron stagnation point.

For the strong guide field case with $J_M E_M$ expected to be the dominant contribution to $\mathbf{J} \cdot \mathbf{E}'$, we note E_M in the 2-D steady case is uniform so the spatial structure of this contribution is given by the structure of J_M . As the guide field increases, electrons are increasingly magnetized. The current is produced where their in-plane bulk flow is small and they are accelerated out of the reconnection plane along the guide field by the reconnection electric field. Therefore, the current should be localized near the electron stagnation point. Thus, as the guide field increases from zero, we expect the region of peaked energy conversion rate $\mathbf{J} \cdot \mathbf{E}'$ to move from midway between the X line and electron stagnation point toward the electron stagnation point (for typical magnetospheric parameters).

The treatment thus far is qualitative, so we turn to a more quantitative approach. To address where $\mathbf{J} \cdot \mathbf{E}'$ is nonzero, we need to find the location of the X line and stagnation points within the diffusion region. Fluid-type conservation laws have been used to predict the absolute and relative locations of the X line and stagnation points (Cassak & Shay, 2007, 2009). However, all the previous work we are aware of on this topic did not include effects of a guide field. This problem needs to be revisited to predict the locations of the X line and stagnation points during reconnection with a guide field.

First, we review the prediction in the zero guide field limit. The distance in the normal direction between the X line and stagnation point is called δ_{XS} . Here we assume the prediction is valid for either species (this has not been verified to our knowledge), so we use a σ subscript to denote i for ions or e for electrons. Combining equations 17, 20, 21, 26, and 28 from Cassak and Shay (2007) gives an expression for δ_{XS} as

$$\frac{\delta_{XS}}{2\delta_\sigma} \sim \frac{n_{1\sigma}B_{L2\sigma}^2 - n_{2\sigma}B_{L1\sigma}^2}{(B_{L1\sigma} + B_{L2\sigma})(n_{1\sigma}B_{L2\sigma} + n_{2\sigma}B_{L1\sigma})}, \quad (1)$$

where $2\delta_\sigma$ is the full thickness of the diffusion region of species σ , n is the density, B_L is the magnitude of the reconnecting component of the magnetic field, the 1 and 2 subscripts refer to the two upstream regions, and the σ dependence on n and B_L reflects that the upstream parameters can be different at the ion and electron diffusion regions. The expression follows solely from conservation of mass and energy in partial volumes of the diffusion regions.

In the absence of a guide field, the thickness δ_σ of the diffusion region is related to the appropriate inertial scale. In asymmetric reconnection, the standard inertial scale needs to be modified due to the presence of the asymmetry (Cassak & Shay, 2009). The result, suitably modified to match the present notation, is

$$\delta_\sigma \sim \frac{1}{2} \left(\sqrt{\frac{B_{L1\sigma}}{B_{L2\sigma}}} + \sqrt{\frac{B_{L2\sigma}}{B_{L1\sigma}}} \right) d_{\sigma,\text{out}} \quad (2)$$

where the asymmetric inertial scale (in SI units) is (Cassak & Shay, 2009)

$$d_{\sigma,\text{out}} = \sqrt{\frac{\epsilon_0 m_\sigma c^2}{q_\sigma^2 n_{\text{out}\sigma}}}, \quad (3)$$

the density of the outflow is (Cassak & Shay, 2007)

$$n_{\text{out}\sigma} \sim \frac{n_{1\sigma}B_{L2\sigma} + n_{2\sigma}B_{L1\sigma}}{B_{L1\sigma} + B_{L2\sigma}}, \quad (4)$$

and q_σ and m_σ are the charge and mass of the species. These expressions are derived by assuming that δ_σ is determined by the particles getting accelerated in the diffusion region by the reconnection electric field and bending in the outflow direction by the reconnected magnetic field. Mathematically,

$$\delta_\sigma \sim \frac{v_{\text{out}\sigma}}{\Omega_{c\sigma}(B_{\text{red}\sigma})}, \quad (5)$$

where the reduced magnetic field is $B_{\text{red}\sigma} = 2B_{L1\sigma}B_{L2\sigma}/(B_{L1\sigma} + B_{L2\sigma})$, the cyclotron frequency is $\Omega_{c\sigma}(B_{\text{red}\sigma}) = |q_\sigma|B_{\text{red}\sigma}/m_\sigma$ (in SI units), and $v_{\text{out}\sigma}$ is the species outflow speed. We expect this to be the asymmetric Alfvén speed $c_{A,\text{asym}\sigma}$ for species σ given by (in SI units) (Cassak & Shay, 2007)

$$c_{A,\text{asym}\sigma}^2 = \frac{B_{L1\sigma}B_{L2\sigma}}{\mu_0 m_\sigma} \frac{B_{L1\sigma} + B_{L2\sigma}}{n_{1\sigma}B_{L2\sigma} + n_{2\sigma}B_{L1\sigma}}. \quad (6)$$

These predictions of diffusion region substructure were confirmed using 2-D two-fluid simulations (Cassak & Shay, 2009) and have some support observationally (Walsh et al., 2014), but we know of no systematic test of these expressions using kinetic simulations.

What changes if there is a guide field? We go through each aspect in turn, starting with equation (1). Since the guide field does not give up energy in the reconnection process, it should not change the energy or mass budget in the fluid sense, so we expect equation (1) to be essentially unchanged merely from the presence of the guide field. However, a guide field is expected to change the thickness δ_σ of the diffusion region (Ek-In et al., 2017; Hesse et al., 2016). Physically, this is because the guide field magnetizes the particles and the gyro-radius decreases with the guide field. For example, for symmetric reconnection, the thickness of the diffusion region is $d_\sigma = c/\omega_{p\sigma}$ (Vasyliunas, 1975), but with a strong guide field the thickness of the layer transitions to the appropriate Larmor radius. This is $\rho_s = c_s/\Omega_{ci}$ for the ions (Rogers & Zakharov, 1995; Zakharov & Rogers, 1992), where $c_s^2 = k_B T_{\text{tot}}/m_i$ is the ion sound speed based on the total temperature T_{tot} , and $\rho_e = v_{\text{th},e}/\Omega_{ce}$ for the electrons (Rogers et al., 2007), where $v_{\text{th},e}^2 = k_B T_e/m_e$ is the electron thermal speed. From this consideration alone, we predict that the absolute separation between the X line and stagnation points decreases with increasing guide field. Consequently, we predict that the absolute distance from the X line to where $\mathbf{J} \cdot \mathbf{E}'$ is nonzero decreases with a guide field.

Given that there is not a theory for the thickness of the diffusion region as a function of guide field even for the symmetric case, we do not attempt a full theory for asymmetric reconnection. However, for small enough guide fields (say, less than 0.1 or 0.2 of the reconnecting field; Swisdak et al., 2005), we expect equations (2) and (3) to provide a reasonable estimate for the thickness δ_σ . For larger guide fields above 0.2 of the reconnecting field, we suspect that $d_{\sigma\text{out}}$ in equation (2) needs to be replaced by the effective Larmor radius:

$$\delta_\sigma \sim \frac{1}{2} \left(\sqrt{\frac{B_{L1\sigma}}{B_{L2\sigma}}} + \sqrt{\frac{B_{L2\sigma}}{B_{L1\sigma}}} \right) \rho_\sigma, \quad (7)$$

and we suggest that by analogy with equation (5), ρ_σ is given by

$$\rho_\sigma = \frac{v_{\text{out}}}{\Omega_{c\sigma}(B_{\text{tot}})}, \quad (8)$$

where B_{tot} is the average of the total magnetic field $(B_L^2 + B_M^2)^{1/2}$ on the two sides and v_{out} is given by $c_{\sigma,\text{asym}}$, the appropriate sound speed for the species σ . By analogy with the antiparallel case, we expect that for the ions, the relevant speed is

$$c_{s,\text{asym}}^2 = \frac{k_B T_{\text{tot,asym}}}{m_i}, \quad (9)$$

where the total temperature is used here (rather than just the ion temperature) (Rogers & Zakharov, 1995; Zakharov & Rogers, 1992) and the asymmetric temperature is (Shay et al., 2014)

$$T_{\text{tot,asym}} = \frac{n_{1i} T_{\text{tot}1} B_{L2i} + n_{2i} T_{\text{tot}2} B_{L1i}}{n_{1i} B_{L2i} + n_{2i} B_{L1i}}. \quad (10)$$

We expect a similar expression to hold for the electrons, with $v_{e,\text{asym}}^2 = k_B T_{e,\text{asym}}/m_e$, where $T_{e,\text{asym}}$ has the same form as equation (10) but with the total temperatures replaced by electron temperatures and the upstream fields and densities evaluated at the electron layer.

The other way that a guide field can change the result from the antiparallel case is that if there is an in-plane pressure gradient, it introduces the diamagnetic drift (Coppi, 1965). When there is a guide field in the M direction and an in-plane pressure gradient in the normal N direction, the X line convects with the electron diamagnetic drift in the outflow L direction (Swisdak et al., 2003). As the diamagnetic drift speed increases, the reconnection rate decreases; if it is bigger than the outflow speed from the electron diffusion region, it can suppress reconnection entirely. We are not aware of any systematic studies of how this physics affects the thickness of the layer, so we offer a possibility here. Motivated by Appendix A in Swisdak et al. (2010), we expect the effective outflow speed to decrease due to diamagnetic effects. Then, we expect δ_σ to decrease due to the v_{out} dependence in the numerator in equations (5) and (8).

To summarize, we suggest that these changes to the antiparallel theory may be useful for estimating the diffusion region substructure for asymmetric reconnection with a guide field. One starts with equation (1) to get the relative separation in the normal direction between the X line and species stagnation point. Then, one uses the appropriate form for δ_σ from equation (2) for low guide field (<0.1) or equation (7) for higher guide fields to get the absolute separation between the X line and species stagnation point. Then, $\mathbf{J} \cdot \mathbf{E}'$ is between X and S_e for weak guide field and moves toward S_e for stronger guide fields (for typical magnetospheric parameters).

Of course, these predictions are presented not with the idea that they are rigorously valid but with the hope that they capture the key physics that potentially explain trends in simulation and observational data. In addition, it should be remembered that these predictions remain confined to the 2-D steady state limit. Three-dimensional effects can be important, including drift wave instabilities that can affect the size and structure of the layer (Daughton, 2013; Davidson & Gladd, 1975; Huba et al., 1977; Le et al., 2017; Roytershteyn et al., 2012; Price et al., 2016, 2017), but this is outside the scope of the present study. We note, however, that drift waves can appear even in 2-D when there is a guide field because the wave number in a system with an out-of-plane M component of a field with a pressure gradient in the normal N direction will be in the outflow L direction, which can be captured in a 2-D system (Beidler & Cassak, 2011).

The discussion so far only takes into account the fluid properties, but kinetic effects that drive the current should be considered as well. In the weak guide field case for typical magnetopause conditions, the magnetosheath electrons crossing the X line and getting accelerated by the normal (Hall) electric field experience

an $\mathbf{E} \times \mathbf{B}$ drift in the M direction, which produces the current (Burch, Torbert, et al., 2016). This is manifested in the electron distribution functions as a crescent-shaped structure (Bessho et al., 2016; Burch, Torbert, et al., 2016; Hesse et al., 2014; Shay et al., 2016). As motivated earlier, this distribution is expected to be clearest midway between the X line and electron stagnation point. As the guide field increases, the electrons become more magnetized and the crescents no longer persist for strong enough guide fields (Hesse et al., 2016). The predictions of this section, while not rigorous, can be tested with kinetic simulations.

3. Particle-In-Cell Simulation Setup

Simulations are performed with the fully kinetic electromagnetic particle-in-cell (PIC) code P3D (Zeiler et al., 2002). The simulations are in a two-dimensional (2-D) domain with periodic boundaries in each direction. (Related 3-D versions of the 16 October 2015 simulation performed here have been discussed in Price et al. (2016, 2017). The code steps particles forward using the relativistic Boris stepper (Birdsall & Langdon, 2004) and steps the electromagnetic fields using the second-order trapezoidal leapfrog (Guzdar et al., 1993); the time step for the electromagnetic fields does not need to be the same as the time step for the particles and is typically smaller.

The simulations are constructed to have asymptotic plasma properties that correspond to the data from three MMS reconnection events as discussed in section 1. We point out that caution is needed about referring to these simulations, or any others, as exact representations of the real events. Most PIC simulations, including the ones here, use unrealistic values for the electron mass and speed of light to make the simulations tractable on modern supercomputers. However, other differences are also important. For example, we are unaware of any simulations of MMS events performed thus far that include the magnetosheath flow in the upstream conditions, and we do not include such flow here. For systems with a large asymmetry, there is reason to believe that the component of the flow in the direction of the reconnecting field does not have much of an impact on the reconnection rate (Doss et al., 2015, 2016); the percentage decrease of the reconnection rate using equation (21) from Doss et al. (2015) for the simulations performed here are 0.04%, 6%, and 20% for the 16 October 2015, 8 December 2015, and 8 September 2015 event simulations, respectively. Therefore, we do not expect much of a change to the location of energy conversion if we include the upstream flow. Flow of course can effect the reconnection site (Nykyri & Otto, 2001), and whether it affects the energy conversion location or rate would be useful to address in future work. We also point out that the constraints of using realistic data often present challenges for resolution, so the simulation domain sizes tend to be rather small, as is the case for the simulations here.

There are other, more fundamental challenges. It is typically the case that the raw satellite data for the asymptotic plasma parameters is not in perfect pressure balance in the MHD sense. It is possible that there are transient effects leading to a temporary lack of pressure balance, but the more likely scenario is that one or more of the measurements may not be accurate. For example, cold particles in the low-density magnetosphere typically are challenging to measure, so the magnetospheric pressure may not be accurate. Therefore, in practice, one must adjust the raw measured satellite data of asymptotic values to ensure that the upstream regions on the two sides of the reconnection site are in pressure balance in the MHD sense to perform a simulation of that event. There are multiple approaches to do this, which introduces some uncertainty. In the simulations performed here, we adjust the asymptotic magnetospheric electron temperature for the 16 October 2015 event and the asymptotic magnetospheric ion temperature for the 8 December 2015 and 8 September 2015 events to ensure that the asymptotic conditions on either side of the reconnection site is in MHD pressure balance.

Finally, there is no universal way to define the upstream parameters from a given set of satellite data. Typically, one finds times slightly before and after when the satellite is on either side of the reconnection region and sees relatively steady conditions, but using data at different times or averaging over different time ranges can lead to different interpretations of the upstream conditions. The parameters chosen for the present study represent our interpretation of the most appropriate upstream parameters, but may not be identical to parameters chosen by others.

The relevant upstream magnetospheric (ms) and magnetosheath (sh) plasma parameters in real units taken from the MMS observations for the 16 October 2015, 8 December 2015, and 8 September 2015 events are given in the first, third, and fifth columns in Table 1, respectively. For the 16 October 2015 event, the simulation is the same as that presented in Burch, Torbert, et al. (2016). For the 8 September 2015 event, it is

Table 1

Upstream Plasma Parameters From the 16 October 2015, 8 December 2015, and 8 September 2015 Reconnection Events Measured by MMS

Quantity	16 Oct 2015		8 Dec 2015		8 Sep 2015	
	Data	Code	Data	Code	Data	Code
$B_{L,sh}$	23 nT	1	15 nT	0.429	15 nT	1
$B_{M,sh}$	2.278 nT	0.099	14 nT	0.4	75 nT	5
n_{sh}	11.3 cm^{-3}	1	7.5 cm^{-3}	0.5	16 cm^{-3}	1
$T_{i,sh}$	320 eV	1.374	533.3 eV	1.313	160 eV	2.288
$T_{e,sh}$	28 eV	0.12	50 eV	0.123	30 eV	0.429
$B_{L,ms}$	39 nT	1.696	35 nT	1	30 nT	2
$B_{M,ms}$	2.278 nT	0.099	12.5 nT	0.357	70 nT	4.667
n_{ms}	0.7 cm^{-3}	0.062	3 cm^{-3}	0.2	6 cm^{-3}	0.375
$T_{i,ms}$	1,800 eV	7.731	553 eV*	1.361	437 eV*	6.248
$T_{e,ms}$	300 eV*	1.288	110 eV	0.271	90 eV	1.287
β_{sh}	2.96	2.96	3.93	3.93	0.20	0.20
β_{ms}	0.39	0.39	0.64	0.64	0.21	0.21

Note. The parameters are the reconnecting magnetic field B_L , the guide field B_M , the plasma density n , the ion temperature T_i , and the electron temperature T_e . The subscripts sh and ms refer to the magnetosheath and the magnetospheric sides of the reconnection site. For each event, parameters extracted from the MMS data are given in real units on the left column, and the same values are provided in normalized units for the simulations in the right column. Magnetospheric temperatures with asterisks denote values that have been adjusted to ensure pressure balance in the MHD sense. The latter part of the table gives associated plasma β on each side.

believed that the event was a secondary process in a Kelvin-Helmholtz instability on the magnetopause flank. While the reconnection is between magnetic fields in the low-latitude boundary layer and the magnetosphere, for simplicity in nomenclature, we continue to refer to the higher-density side as the magnetosheath even though it does not represent the actual magnetosheath. Magnetospheric temperatures in the table with asterisks mark those that were adjusted to enforce pressure balance. The second, fourth, and sixth columns give the parameters normalized for use in the simulations. For the 16 October 2015 and 8 September 2015 event simulations, magnetic fields and densities are normalized to the magnetosheath reconnecting field $B_0 = B_{L,sh}$ and density $n_0 = n_{sh}$. For the 8 December 2015 event simulation, magnetic fields are normalized to the magnetospheric reconnecting magnetic field $B_0 = B_{L,ms}$, and densities are normalized to $n_0 = 2n_{sh}$. However, all quantities in this study except otherwise noted are converted to be in units normalized to magnetosheath quantities. Thus, length scales are in terms of the ion inertial length $d_{i,sh}$, time scales are in terms of $\Omega_{i,sh}^{-1}$ based only on the reconnecting component of the magnetic field $B_{L,sh}$, current density scales are in

terms of $J_{sh} = B_{L,sh} / \mu_0 d_{i,sh}$, and the rate of work done by electric fields are in terms of $J_{sh} E_{sh} = J_{sh} B_{L,sh} c_{AL,sh}$, where $c_{AL,sh} = B_{L,sh} / (\mu_0 m_i n_{sh})^{1/2}$ is the Alfvén speed based on magnetosheath quantities. Converting these normalized units into real units for the three event simulations can be done with the values given in Table 2.

Each of the simulations have initial conditions to enforce pressure balance in the MHD sense across the whole current sheet. The reconnecting field B_L , the guide field B_M , and the electron and ion temperatures T_e and T_i all have double \tanh profiles with a length scale given by w_0 of 1 for the 16 October 2015 and 8 September 2015 event simulations and 1.2 for the 8 December 2015 event simulation. In particular, the guide field need not be the same on the two sides of the diffusion region. The density profile is then chosen to make the system in MHD pressure balance, and only one species (protons) is assumed. As is typical, these asymmetric initial conditions do not represent an equilibrium solution to the Vlasov equation (Pritchett, 2008). Consequently, the 16 October 2015 event simulation rings initially

Table 2

Normalizations to Convert the Numbers Given in Code Units to Real Units for the Three Event Simulations in the Present Study

Quantity	16 Oct 2015	8 Dec 2015	8 Sep 2015
$d_{i,sh}$ (km)	67.8	83.2	57.0
$\Omega_{i,sh}^{-1}$ (s)	0.452	0.695	0.696
$c_{AL,sh}$ (km/s)	150	120	81.9
$c_{Atot,sh}$ (km/s)	151	164	418
J_{sh} ($\mu\text{A}/\text{m}^2$)	0.270	0.287	0.210
$(\mathbf{J} \cdot \mathbf{E})_{sh}$ (nW/m^3)	0.928	0.258	0.257
E_{norm} (mV/m)	3.435	1.80	1.23

Note. $\Omega_{ci,sh}^{-1}$ is based only on the reconnecting field $B_{L,sh}$, not the total magnetic field.

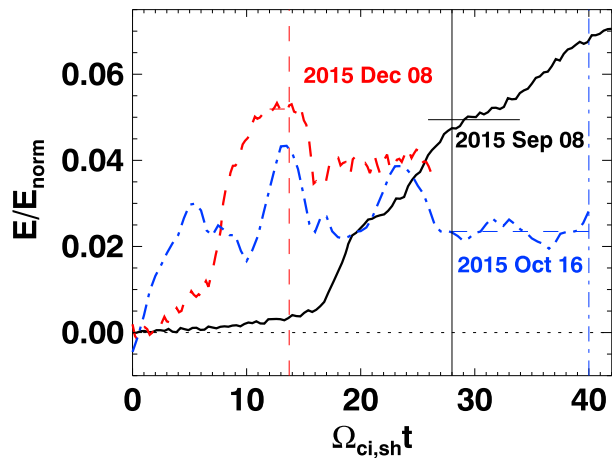


Figure 1. Reconnection rate E in the PIC simulations normalized to the theoretical normalization E_{norm} from equation (12) for each simulation as a function of time t normalized to the appropriate ion cyclotron frequency $\Omega_{\text{ci,sh}}$ based on the magnetosheath reconnecting field $B_{\text{L,sh}}$. The simulation for 16 October 2015 (guide field 0.1) is denoted by the dash-dotted blue line, 8 December 2015 (guide field 1) is the dashed red line, and 8 September 2015 (guide field 5) is the solid black line. Associated vertical lines mark the time at which other plots are taken, and horizontal lines show the time range over which the reconnection rate is taken as steady. To convert to real units, see the conversion factors in Table 2.

X line, are provided as supporting information. In each, the perturbation used to initiate reconnection grows and primary islands are generated. The X lines in the 16 October 2015 (low guide field) and 8 September 2015 (high guide field) event simulations do not drift appreciably in the outflow L direction. However, the X line in the 8 December 2015 (medium guide field) event simulation clearly drifts in the L direction, moving $4.4 d_{j0}$ in a time of $62 \Omega_{c0}^{-1}$ implying an L velocity of $0.07 c_{A0}$. We attribute this to diamagnetic drifts as discussed in section 2; the predicted electron diamagnetic drift speed v_{*e} for the parameters in use is $0.06 c_{A0}$, in good agreement with the measured speed.

The reconnection rates of the three event simulations are plotted as a function of time in Figure 1. The 16 October 2015, 8 December 2015, and 8 September 2015 event simulations are shown as the blue dash-dotted, the red dashed, and the black solid lines, respectively. The reconnection rate E is obtained in the standard way for periodic domains using the flux function ψ as the time rate of change of magnetic flux between the X line (saddle point of ψ) and the O line (extremum of ψ). The reconnection electric field is balanced at the X line by the electron inertia term for all three simulations (not shown), with an oppositely directed contribution of the electron pressure divergence in the 16 October 2015 and 8 December 2015 event simulations.

To make a more meaningful comparison between the simulations, the reconnection rates are normalized using the formalism in Cassak and Shay (2007). We make this choice even though the theory does not include the effects of a guide field, so it does not include the decrease in the reconnection rate due to diamagnetic effects (Swisdak et al., 2003) and therefore is not expected to be correct for these events. The predicted reconnection rate E_{asym} in terms of the magnetosheath and magnetospheric reconnecting fields (in SI units) is

$$E_{\text{asym}} = \frac{2B_{L1}B_{L2}}{B_{L1} + B_{L2}} c_{A,\text{asym},i} \frac{\delta}{L}, \quad (11)$$

where $c_{A,\text{asym},i}$ is the asymmetric Alfvén speed given in equation (6). The typical value for δ/L in antiparallel symmetric (Liu et al., 2017; Shay et al., 1999) and asymmetric (Cassak & Shay, 2008; Malakit et al., 2010) reconnection is close to 0.1. We show the simulated reconnection electric fields normalized to

$$E_{\text{norm}} = \frac{2B_{L1}B_{L2}}{B_{L1} + B_{L2}} c_{A,\text{asym},i}, \quad (12)$$

as the system adjusts to being out of equilibrium. A similar effect is seen for the 8 December 2015 event simulation, but with a much smaller amplitude. Almost no ringing is seen in the 8 September 2015 event simulation. We suspect that the larger the guide field, the closer these events are to equilibrium and the less the system rings.

The electron mass in all three event simulations is $m_e = m_i/100$. The speed of light normalized to the reference Alfvén speed $c_{A0} = B_0/(\mu_0 m_i n_0)^{1/2}$ in the three simulations is $c/c_{A0} = 15$ for 16 October 2015, $c/c_{A0} = 25$ for 8 December 2015, and $c/c_{A0} = 20$ for 8 September 2015. The domain size for all three simulations is 40.96×20.48 in units of $d_{j0} = (\epsilon_0 m_i c^2 / e^2 n_0)^{1/2}$. The grid scale in both directions is $0.01 d_{j0}$ for 16 October 2015 and 8 December 2015, but is 0.05 for 8 September 2015. The larger guide field requires a smaller grid to properly resolve the electron Larmor radius. Each simulation used an average of 500 particles per grid cell with equal weight. The particles are stepped forward with a time step small enough to resolve plasma waves, the cyclotron time, and electron Alfvén waves. The electromagnetic fields have a time step half the size to resolve light waves. A coherent magnetic perturbation of amplitude $0.1 B_0$ is used to initiate reconnection in the double tearing configuration.

4. Results

First, we consider the large-scale evolution of reconnection in the three simulations. Animations of the time evolution of the out-of-plane current density J_M for the three event simulations, zoomed in to a region near the

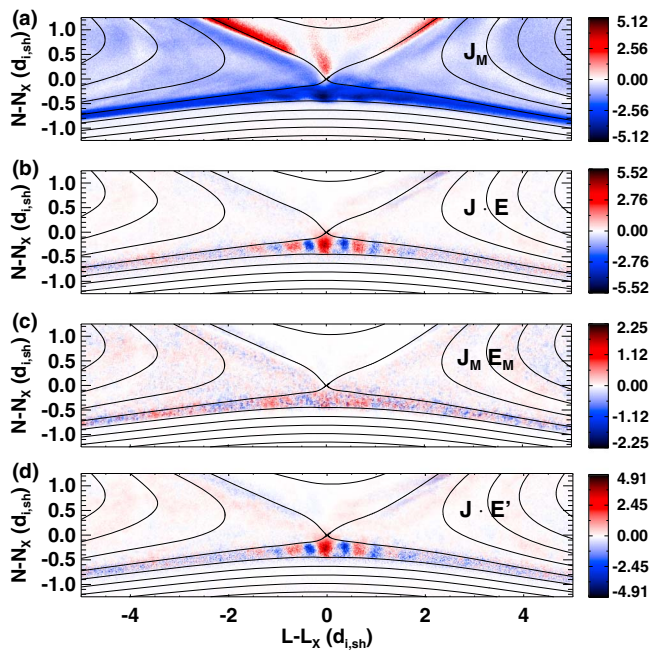


Figure 2. Energy conversion in the PIC simulations for the 16 October 2015 event at $\Omega_{ci,sh} t = 40$. (a) Out-of-plane current density J_M , (b) rate of work done by the electric field $\mathbf{J} \cdot \mathbf{E}$, (c) rate of work done by the electric field $J_M E_M$ only associated with the out-of-plane direction, and (d) rate of work done by the electric field in the reference frame of the electrons $\mathbf{J} \cdot \mathbf{E}'$ as a function of L and N relative to the X line. To convert to real units, see the conversions in Table 2.

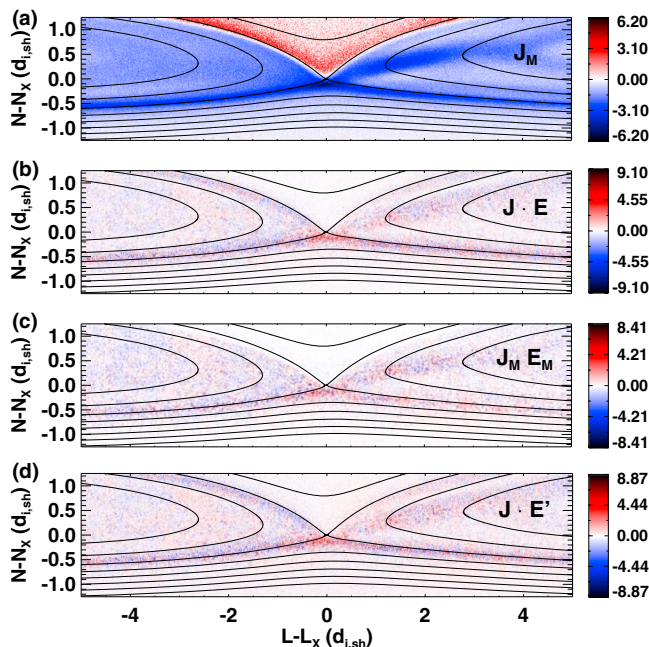


Figure 3. As in Figure 2 but for the 8 December 2015 event PIC simulation at $\Omega_{ci,sh} t = 13.728$.

which is E_{asym} divided by δ/L . Thus, the reference value for E/E_{norm} is 0.1; if the theory perfectly described the simulation results, the rate would be close to 0.1. The corresponding E_{norm} values converted to real units are given in Table 2.

The 16 October 2015 (guide field 0.1) and 8 December 2015 (guide field 1) event simulations show the reconnection rate increasing from zero and achieving a relatively steady state. The ringing in the 16 October 2015 event simulation is because the initial conditions are not in a kinetic equilibrium, as discussed in section 3. Horizontal lines are plotted at $\Omega_{ci,sh} t$ of 28 to 40 for 16 October 2015 and 12.012 to 14.586 for 8 December 2015 denoting where a steady state is reached. For the 8 September 2015 (guide field 5) event simulation, the reconnection rate increases, but it does not turn over to a steady state in the time for which the simulation is performed. It is suspected that a larger simulation domain would be needed to reach a steady state, but this is not carried out for the present study because it is prohibitively expensive due to the large guide field and is not expected to impact the key results. A horizontal line from $\Omega_{ci,sh} t$ of 25.9 to 33.95 denotes where we take as range to estimate the reconnection rate. The vertical lines at $\Omega_{ci,sh} t = 40, 13.728,$ and 28 denote times at which forthcoming plots are taken.

The normalized reconnection rates averaged over the given times are $E/E_{norm} = 0.0235, 0.0519,$ and 0.0494 for the 16 October 2015, 8 December 2015, and 8 September 2015 event simulations, respectively. Converting the simulated reconnection rates to real units using E_{norm} from Table 2 gives $0.17, 0.21,$ and 0.074 mV/m, respectively. We will use these in section 5 to compare to observations.

We now investigate the rate at which work is done on the particles by the electric field at the times denoted by vertical lines in Figure 1. For each event simulation, shown in Figures 2–4, we plot (a) the out-of-plane current density J_M , (b) the rate of work done by the electric field in the simulation reference frame $\mathbf{J} \cdot \mathbf{E}$, (c) the contribution solely from the out-of-plane part $J_M E_M$, and (d) the rate of work done by the electric field in the reference frame of the electrons $\mathbf{J} \cdot \mathbf{E}' = \mathbf{J} \cdot (\mathbf{E} + \mathbf{v}_e \times \mathbf{B})$. Each are plotted as a function of L and N in a small domain localized around the X line with axes that have been shifted so that the X line is at the origin. No smoothing or time averaging has been carried out in making these plots. The color table has red as positive, white as zero, and blue as negative, and in-plane magnetic field lines are overplotted in black. The color tables on the three plots relating to the rate of work done are not the same for each event simulation. The latter plot is the nonrelativistic form of the D_e parameter discussed by Zenitani et al. (2011); it is commonly called the “dissipation parameter,” but nonzero value for D_e may be associated with dissipation but it is not necessarily so. This is because the acceleration of a charged particle in an electric field is reversible unless the particle undergoes collisions. For this reason, we refer to $\mathbf{J} \cdot \mathbf{E}'$ as “the rate of work done by the electric field” or the “energy conversion rate” instead of “dissipation.”

These simulation data are shown in Figure 2 for the 16 October 2015 event at $\Omega_{ci,sh} t = 40$. There is interesting structure in $\mathbf{J} \cdot \mathbf{E}$ and $\mathbf{J} \cdot \mathbf{E}'$; the rate of work done oscillates between positive and negative in a band near the magnetospheric separatrix. These structures persist in other simulations with up to 3,500 particles per grid, so we believe this is physical rather than numerical. We discuss the physical mechanism causing this structure in a separate paper. Here we focus instead on its location relative to the X line

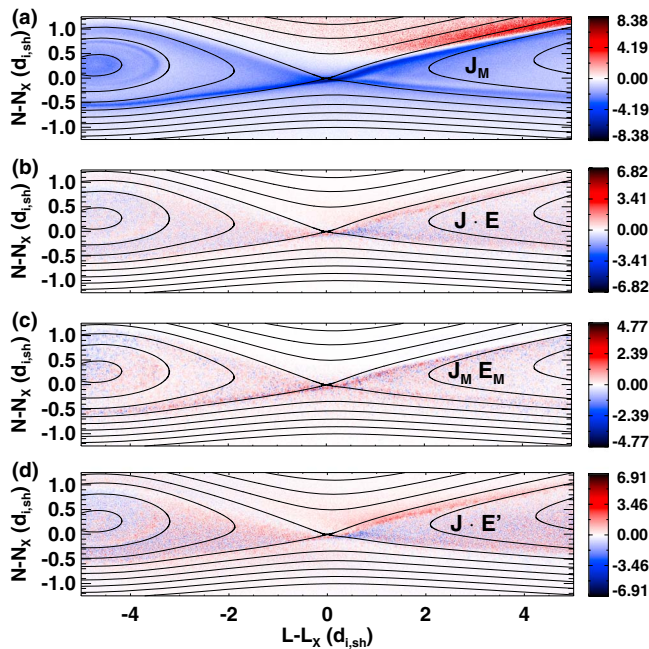


Figure 4. As in Figure 2 but for the 8 September 2015 event PIC simulation at $\Omega_{ci,sh}t = 28$.

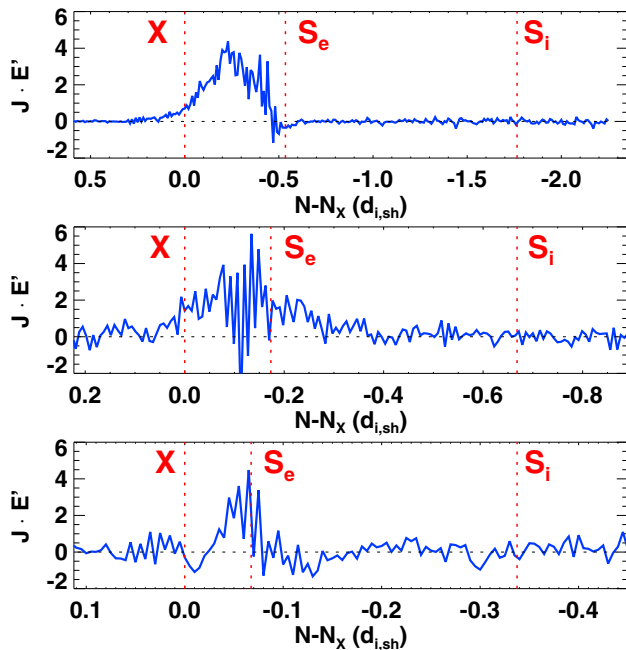


Figure 5. Cut in the N direction of $\mathbf{J} \cdot \mathbf{E}'$ through the X line for the (top) 16 October 2015, (middle) 8 December 2015, and (bottom) 8 September 2015 PIC simulations, at $\Omega_{ci,sh}t = 40, 13.728$, and 28 , respectively. The vertical dashed lines mark the X line X and the locations in the same cut of the electron S_e and ion S_i flow reversals (stagnation points). The horizontal axes are rescaled in the three plots so that the X line and the ion flow reversal line up. Data are presented in normalized units given in Table 2.

and stagnation point. We also point out that by comparing Figures 2c and 2d, the dominant contribution to $\mathbf{J} \cdot \mathbf{E}'$ is not due to the portion along the X line but rather is due to the in-plane dynamics. This is consistent with the discussion of section 2.

Similar plots for the 8 December 2015 and 8 September 2015 event simulations are shown at $\Omega_{ci,sh}t = 13.728$ and 28 , respectively, in Figures 3 and 4. The signals in these two simulations are smoother, without the oscillations seen in the 16 October 2015 event simulation. By comparing Figures 3c and 3d and Figures 4c and 4d, we see that the dominant contribution to $\mathbf{J} \cdot \mathbf{E}'$ is from $J_M E_M$, as anticipated in section 2. It is challenging to clearly ascertain where the energy conversion rate is nonzero from these plots, so we take cuts of $\mathbf{J} \cdot \mathbf{E}'$ in the vertical direction N through the X line for each.

The results are shown in Figure 5 for (top) 16 October 2015, (middle) 8 December 2015, and (bottom) 8 September 2015. The vertical dashed lines mark the X line X , the electron stagnation point S_e , and the ion stagnation point S_i . A number of important points warrant further comment. First, while the location of the X line is Galilean reference frame independent (in a nonrelativistic system as is the case here), the stagnation points are not. Many studies have plotted the stagnation point in the reference frame of the simulation, but if the X line is in motion, this is not the appropriate reference frame to determine properties of the reconnection since the reconnection electric field is not uniform in that frame (Mozer et al., 2002). In asymmetric reconnection, the X line typically convects in the normal N direction toward the side with the stronger magnetic field (Cassak & Shay, 2007, 2009) because it is energetically favorable compared to the X line remaining stationary and bending the stronger field. This happens to greater or lesser extent in all of the simulations treated here, so all of the data are shifted into the reference frame of the moving X line. To do so, we plot the out-of-plane component of the convection term $-(\mathbf{v}_i \times \mathbf{B})_M$ from the generalized Ohm's law in a cut along the normal direction through the X line. Using the expressions in Cassak and Shay (2009) and Mozer et al. (2002), we add a uniform bulk flow in the normal direction until the upstream values of the convection electric field on the two sides of the diffusion region are approximately equal; this determination is done by eye. The species velocities are then measured in this moving reference frame; the magnetic fields, densities, and pressures are unchanged by this change of reference frame. Locations where the bulk flow reverses along the cut normal to the X line for each species are identified as the stagnation point. Note, this is prohibitively difficult when the number of particles per grid is small because of particle noise, so having high enough particles per grid cell as done here is crucial to carry out this procedure. The distance the location of the stagnation point shifts by going into the moving reference frame for a given system depends on the extent of the asymmetry; whether it is necessary should be assessed for each individual case.

A second point is that the term “stagnation point” is nuanced. Formally, the stagnation point is the single point where the in-plane bulk velocity of a species vanishes. In a vertical cut through the X line, there is a location where the vertical bulk velocity goes through zero, which is what we are labeling the stagnation point. However, there may be horizontal flow at this point. Indeed, it has been found that the true stagnation point can be displaced in the horizontal L direction when there is a guide field (M. Hesse et al., presentation at the 2016 Mini-GEM meeting). We choose to still refer to the flow reversal in this cut as the stagnation point. The 2-D plots in Figures 3 and 4 show that the location and magnitude of $\mathbf{J} \cdot \mathbf{E}$ and $\mathbf{J} \cdot \mathbf{E}'$

Table 3

Predicted Quantities (in Units Normalized to the Properties in the Magnetosheath) in the Calculation Leading Up to the Separation Between the X line X and the Stagnation Point S_σ , Both for Ions and Electrons

Quantity	16 Oct 2015	8 Dec 2015	8 Sep 2015
$\frac{n_1 B_{L2i}^2 - n_2 B_{L1i}^2}{(B_{L1i} + B_{L2i})(n_1 B_{L2i} + n_2 B_{L1i})}$	0.594	0.553	0.508
$v_{\text{out}} (c_{\text{AL,sh}})$	$c_{\text{A,asym,i}} = 1.61$	$c_{\text{s,asym,i}} = 1.44$	$c_{\text{s,asym,i}} = 2.17$
$\Omega_{\text{ci}} (\Omega_{\text{ci,sh}})$	1.26 (based on $B_{\text{red,i}}$)	2.01 (based on B_{tot})	5.09 (based on B_{tot})
$\delta_i = v_{\text{out}} / \Omega_{\text{ci}} (d_{i,\text{sh}})$	1.28	0.716	0.426
$\delta_{\text{XS}_i} = 2\delta_i (\text{Row 1}) (d_{i,\text{sh}})$	1.52	0.792	0.216
$\delta_{\text{XS}_i} (d_{i,\text{sh}})$ (Simulations)	1.765	0.668	0.3375
$v_{\text{out,e}} (c_{\text{AL,sh}})$	$c_{\text{A,asym,e}} = 16.1$	$v_{\text{e,asym}} = 20.8$	$v_{\text{e,asym}} = 7.50$
$\Omega_{\text{ce}} (\Omega_{\text{ce,sh}})$	126 (based on $B_{\text{red,i}}$)	201 (based on B_{tot})	509 (based on B_{tot})
$\delta_e = v_{\text{out,e}} / \Omega_{\text{ce}} (d_{i,\text{sh}})$	0.128	0.103	0.0147
$\delta_{\text{XS}_e} = 2\delta_e (\text{Row 1}) (d_{i,\text{sh}})$	0.152	0.114	0.014
$\delta_{\text{XS}_e} (d_{i,\text{sh}})$ (Simulations)	0.535	0.173	0.0675
$\frac{1}{2} \left(\sqrt{\frac{B_{L1}}{B_{L2}}} + \sqrt{\frac{B_{L2}}{B_{L1}}} \right) d_{\text{e,out}} (d_{i,\text{sh}})$	0.128	0.120	0.119

Note. Normalizations to convert these to real units are in Table 2. The top line is the right-hand side of equation (1). The second line is what is referred to as v_{out} in section 2, which is $c_{\text{A,asym,i}}$ for low guide field and $c_{\text{s,asym,i}}$ for strong guide field. The third line is the appropriate ion cyclotron frequency as discussed in section 2; based on the reduced magnetic field for low guide field and the average guide field for the strong guide field. The fourth line is the predicted half thickness of the diffusion region, and the fifth line is the predicted absolute distance between X and S_i . The sixth line is the measured value of δ_{XS_i} in the simulations, as seen in Figure 5. Below the horizontal line, the calculations are repeated for the electron layer. The last line has the prediction using the inertial scale instead of the thermal Larmor radius, showing that the thermal Larmor radius better agrees with the results.

are similar within a small range in L around the X line, which justifies the use of the data along a vertical cut through the X line.

We are now prepared to analyze the results. First, we discuss both the relative and absolute structure of the dissipation region and the location where the energy conversion rate is nonzero, starting with the structure. We first consider the ion scales. Figure 5 is plotted such that the horizontal axes have been scaled to make the X lines and ion stagnation points S_i line up in the three panels. For each simulation, we calculate the prediction for δ_{XS_i} using the expressions in section 2. The intermediate steps in the calculations for the ion scale structure are provided in Table 3. The top row in Table 3 gives the right-hand side of equation (1). For all three cases, the right-hand side of equation (1) is predicted to be between 0.5 and 0.6, meaning that the ion stagnation point is predicted to be about half the diffusion region thickness on the magnetospheric side of the X line for each event simulation. The second and third rows in Table 3 give v_{out} and Ω_{ci} for the three simulations, using $c_{\text{A,asym,i}}$ and $\Omega_{\text{ci}}(B_{\text{red}\sigma})$ for the 16 October 2015 low guide field case but $c_{\text{s,asym,i}}$ and $\Omega_{\text{ci}}(B_{\text{tot}})$ for the two higher guide field cases. The fourth row of the table gives their ratio, which is a prediction for the half thickness of the ion diffusion region δ_i . The fifth row of the table gives the prediction for the absolute distance from the X line to the ion stagnation point δ_{XS_i} using equation (1). The results for δ_i and δ_{XS_i} show strong decreases in the absolute thickness with increasing guide field, reflecting that the particles have smaller Larmor radii.

The results from the PIC simulations for the values of δ_{XS_i} , extracted from Figure 5, are given in the sixth row of Table 3. While perfect absolute agreement is not expected given the crudeness of the predictions, we see that the trend of reduced thickness with increasing guide field is nicely described. As a reminder, diamagnetic effects are not included here, though they are expected to be important for the 8 December 2015 event, potentially making the diffusion region thinner by decreasing the outflow speed v_{out} that comes into the numerator of ρ_σ in equation (8). The results are suggestive that, for these event simulations, it is reasonably the case that the large changes in the absolute location of the X line and ion stagnation point are mostly attributable to the role of the guide field in making the diffusion region thinner.

For the separation of the X line and the electron stagnation point, similar calculations are performed in the lower portion of Table 3. For the right-hand side of equation (1), we take the upstream magnetic fields

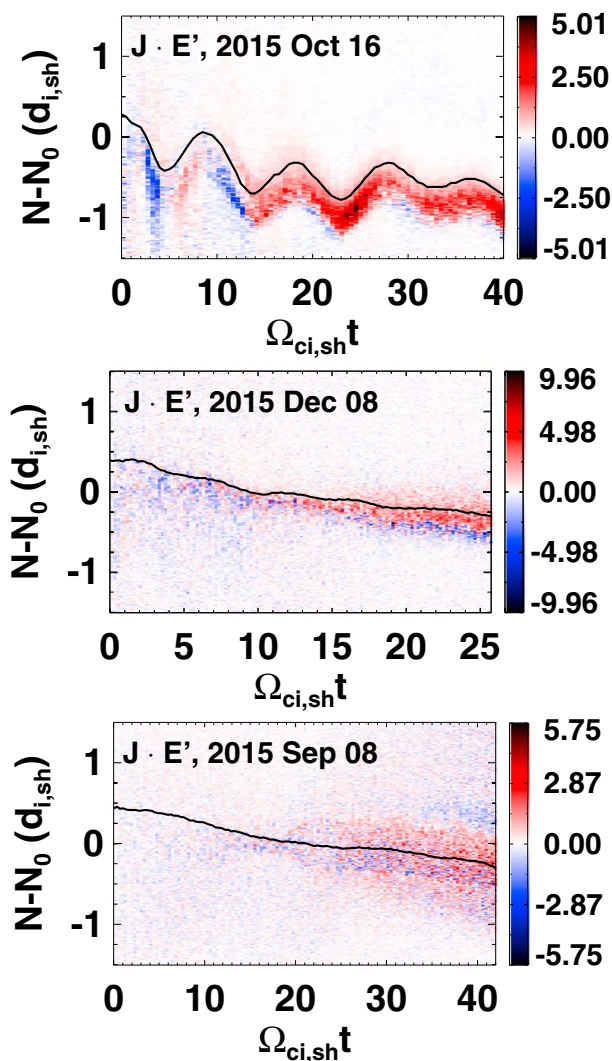


Figure 6. Stack plots of a cut in the N direction through the X line of $\mathbf{J} \cdot \mathbf{E}'$ as a function of time t normalized to $\Omega_{ci,sh}$ for the (top) 16 October 2015, (middle) 8 December 2015, and (bottom) 8 September 2015 PIC simulations. The N axis has been shifted by N_0 , the center of the current sheet at the simulation's initialization. The black curve is the location of the X line. Data are presented in normalized units given in Table 2.

each plot marks the X line. The top plot for the 16 October 2015 event simulation vividly shows the ringing of the current sheet discussed in section 3. As it settles down at late times, we see that indeed the region of nonzero $\mathbf{J} \cdot \mathbf{E}'$ is consistently about the same distance on the magnetospheric side for all late times. The red color indicates that $\mathbf{J} \cdot \mathbf{E}'$ is positive, so energy is going from the electric field to the particles. Some ringing is seen in the middle plot for the 8 December 2015 event simulation. The main signal is the positive $\mathbf{J} \cdot \mathbf{E}'$ just to the magnetospheric side of the X line. Interestingly, there is a band of blue color on the magnetospheric side of the X line, corresponding to a generator where energy goes from the particles to the electric field. This may be a result of not going into the appropriate reference frame with a uniform reconnection electric field, but we do not pursue this further as it is not our main goal. For the bottom plot for the 8 September 2015 event simulation, the red signal is near the X line region, closer to it than the other two simulations in absolute distance. Interestingly, it appears as though the red region is broader, though this may just be due to noisiness of the signal, and is nonzero on both sides of the X line at late times. We conclude from the three panels that the results obtained here are not just valid at the single time investigated here but are consistently valid as a function of time.

and densities to be the same as at the ion layer even though this is not expected to be the case. We suspect, without testing, that the asymmetry at the electron layer is larger than at the ion layer, so these predictions might actually be a bit smaller than they should be. The first five rows below the midline in Table 3 show results of analogous calculations for electrons. For the 16 October 2015 low guide field event simulation, the prediction does not agree with the simulations, which are over a factor of 3 larger than predicted. We suspect the disagreement is caused by the structures present on the magnetospheric side of the X line as discussed earlier in this section. For the large guide field case, the theory, which assumes that the thickness is controlled by the thermal gyroradius, reasonably captures the observed trend, though again the absolute agreement is not great. For completeness, we include a sixth line in the table containing the prediction if the electron layer thickness is governed by the electron inertial scale instead of the thermal gyroradius. These predictions do not capture the trend, which suggests that the electron thermal gyroscale is the more appropriate scale as we expected, at least for the present simulations.

We also note in Figure 5 that there is a weak systematic effect that the relative size of δ_{X_S} decreases slightly with increasing guide field. Interestingly, this trend is qualitatively consistent with the predicted relative scales, given in the top line of Table 3, which decrease from 0.594 to 0.508 for the simulations with weak and strong guide fields. To summarize the findings so far, the predictions from section 2 do a reasonable job of predicting trends in the location of the positions of the X line and electron and ion stagnation points.

Now, we turn from the structure of the diffusion region to the impact of the guide field strength on where the energy conversion rate is nonzero. In all three cases, we clearly see that the peak is between the X line X and electron stagnation point S_e , as predicted. There is also a systematic effect due to the guide field. The peak is essentially midway between X and S_e for the low guide field 16 October 2015 event simulation, and approaches S_e as the guide field is increased in the 8 December 2015 and 8 September 2015 event simulations. This is consistent with the theoretical expectations as discussed in section 2.

It is important to confirm that the results obtained here are not only valid at the particular time being considered. This is addressed in Figure 6. The three panels are stack plots of $\mathbf{J} \cdot \mathbf{E}'$ in a vertical cut through the X line (which need not be stationary), stacked as a function of time. The black curve in

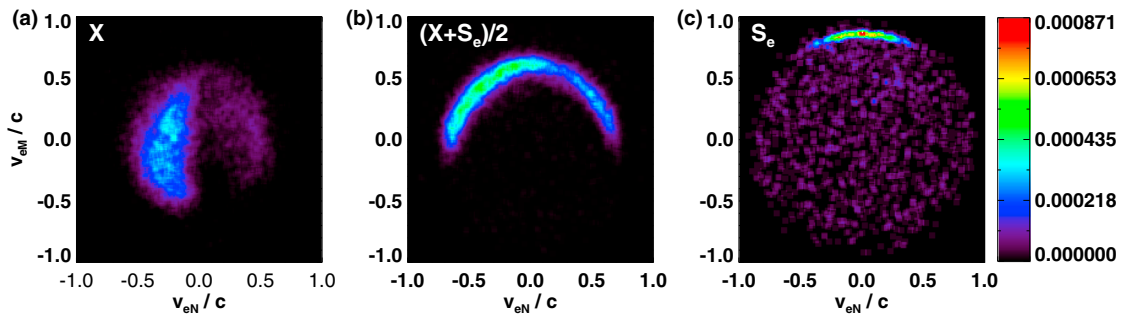


Figure 7. Reduced distribution functions in arbitrary units in the $v_M - v_N$ plane for the PIC simulations of the 16 October 2015 event at $\Omega_{ci,sh}t = 40$. They are evaluated at (a) the X line X , (b) halfway between the X line and the electron flow reversal point S_e in the N cut through the X line, and (c) at the electron flow reversal point S_e .

Finally, we put the results for where $\mathbf{J} \cdot \mathbf{E}'$ is peaked in context of the kinetic physics driving the current by looking at electron distribution functions. Each plot in Figures 7–9 shows the reduced distribution function in the $v_{eM}v_{eN}$ plane at the same time as the 2-D plots shown previously. The panels are evaluated at (a) the X line X , (b) halfway between the X line and electron stagnation point $(X + S_e)/2$, and (c) at the electron stagnation point S_e . Spatial averaging is done over a 6 grid cell by 6 grid cell region in L and N centered at the point in question for all three event simulations.

Results for the 16 October 2015, 8 December 2015, and 8 September 2015 event simulations are shown in Figures 7, 8, and 9, respectively. For the 16 October 2015 event simulation with weak guide field, the middle plot shows clear evidence of the crescent-shaped distribution seen in simulations (Hesse et al., 2014) and in MMS observations (Burch, Torbert, et al., 2016). There is a small crescent-like shape at S_e , but it seems as though the crescent distribution consistent with driving the main part of the current is closer to halfway between X and S_e rather than at S_e . This is consistent with the finding that J_M is peaked between X and S_e for the 16 October 2015 event simulation.

For the 8 December 2015 event simulation in Figure 8 with moderate guide field, the vestige of a crescent is visible in all three plots, but it is small compared to the rest of the distribution. For the large guide field event simulation in Figure 9, no detectable crescent is seen. The results are qualitatively consistent with the predictions by Hesse et al. (2016) that the crescents disappear for large guide field. In the context of the kinetic cause of the current density, there is clearly a beam offset from the origin in the distribution function at all three locations, but it is dominant at S_e . This is consistent with the peak in the energy conversion rate being close to S_e for increasing guide fields and confirms the expectation that the current is closer to the electron stagnation point for larger guide fields, where the current is generated by electrons accelerating along the guide magnetic field due to the parallel reconnection electric field.

5. Comparison to MMS and AMPERE Observations and Global Simulations

We now compare the theory and event PIC simulation results to local reconnection observations from MMS data, the inferred global and local picture from the Active Magnetosphere and Planetary Electrodynamics Response Experiment (AMPERE), and to a global magnetospheric resistive-MHD simulation. The MMS data

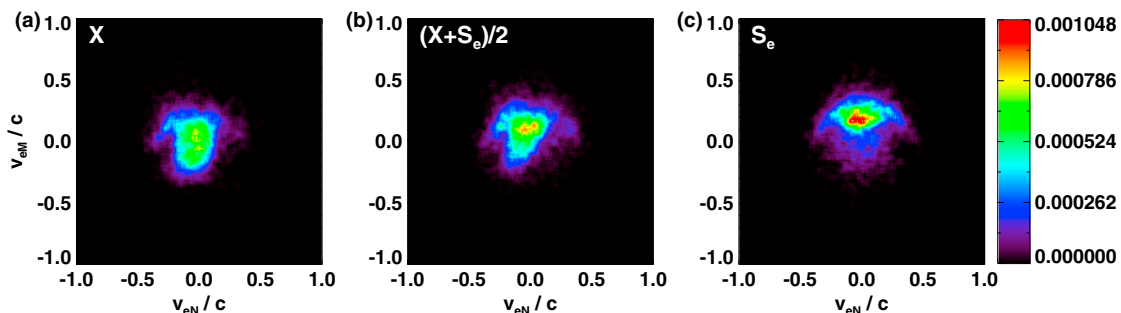


Figure 8. As in Figure 7 but for the 8 December 2015 PIC simulation at $\Omega_{ci,sh}t = 13.728$.

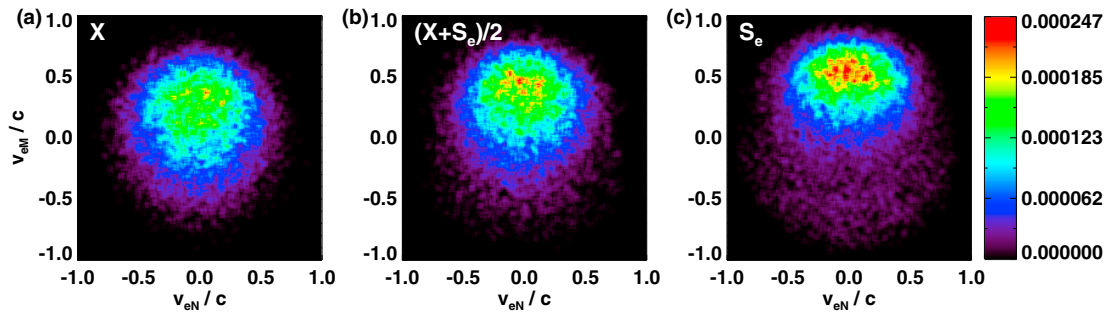


Figure 9. As in Figure 7 but for the 8 September 2015 PIC simulation at $\Omega_{ci,sh}t = 28$.

are taken from Burch, Torbert, et al. (2016) (16 October 2015), Burch and Phan (2016) (8 December 2015), and Eriksson, Wilder, et al. (2016) (8 September 2015). The energy conversion rate from these three events is synthesized in the companion paper (Genestreti et al., 2017).

We first consider the reconnection electric field. As stated in section 4, the simulated reconnection rates E_{sims} when converted to real units are 0.17, 0.21, and 0.074 mV/m. We compare that to what we have for theoretical predictions from Cassak and Shay (2007). That theory was for antiparallel 2-D asymmetric reconnection with no upstream flow, while the real events are 3-D, have a guide field, and have upstream flow. So, these should just be interpreted as a guideline rather than a precise prediction. The results, using equations (11) and (6) and the upstream parameters from Table 1 are $E_{theory} = 0.70, 0.42, \text{ and } 0.26$ mV/m. It is known that this theory tends to overpredict the rate in PIC simulations by a factor of 2 (Malakit et al., 2010), so if we adjust for this, we get 0.35, 0.21, and 0.13 mV/m. The theoretical predictions are in reasonable agreement with the simulations, within a factor of 2 for each simulation.

We also compare the results to global magnetospheric magnetohydrodynamic (MHD) simulation using solar wind conditions from the 16 October 2015 event. The global magnetospheric simulation employs the Block Adaptive Tree Solarwind Roe-type Upwind Scheme (BATS-R-US) MHD code (De Zeeuw et al., 2000; Gombosi et al., 2000; Powell et al., 1999) coupled with the ionospheric electrodynamics model and is performed at NASA's Goddard Space Flight Center's Community Coordinated Modeling Center (CCMC). The MHD simulation domain is $-255 < x < 33, -48 < y < 48, \text{ and } -48 < z < 48$ and uses a resolution of 0.125 throughout the region $-15 < x, y, z < 15$, where distances and grid cell size are measured in Earth radii R_E . The coordinate system is Geocentric Solar Magnetic. The global simulation includes a uniform explicit resistivity $\eta/\mu_0 = 6.0 \times 10^{10} \text{ m}^2/\text{s}$. Although the magnetopause is known to be collisionless, including an explicit resistivity allows for reproducible results that are independent of the numerics (e.g., Komar et al., 2013). The parameters in the solar wind are generated using the CCMC's Runs on Request service and automatically generated from 1 min OMNI measurements propagated from L1 to the MHD boundary at $x = 33 R_E; B_x = 0$ nT and is updated as a function of time. The ionosphere is modeled via conservation of electric charge from the currents of the MHD simulation at $3.5 R_E$ mapped to the ionosphere at a radial distance of $1.017 R_E$. Representative auroral Pederson and Hall conductances are determined from an $F_{10.7}$ index of 108.4 solar flux units to the ionospheric electric field \mathbf{E} on a 181×181 geomagnetic latitude and longitude grid.

The simulated polar cap potential in the Northern Hemisphere 11 min after the MMS crossing (13:18:00) is plotted in Figure 10 (top). The delay by 11 min is to make a direct comparison to the observations, which experience a delay between the reconnection event at 13:07 and the time that the signal from it is detected in the ionosphere. We point out that direct comparisons of this sort are nontrivial because of the way the codes are initialized, but we find that the numerical results are not strongly time dependent and therefore represent a reasonable comparison. The cross polar cap potential Φ_{CPCP} is 59.8 kV. The X line (technically the magnetic separator, but they are essentially the same for our purposes) is traced using the techniques of Komar et al. (2013); Figure 11 shows the magnetopause in green dots and the separator in blue dots at 13:07, the time of the MMS crossing. The red dot shows the position of MMS at the time of its actual crossing, which is within $1 R_E$ of the simulated X line. The reconnection electric field, calculated as the electric field ($\eta J_{||} = \eta \mathbf{J} \cdot \hat{\mathbf{M}}$) parallel to the separator (X line) (Komar & Cassak, 2016), is plotted as a function of distance along the separator in units of Earth radii R_E at 13:07 in Figure 12. Zero is the subsolar point, and the vertical line at $-9 R_E$ denotes the location of closest approach to the separator by MMS. The reconnection rate at that location

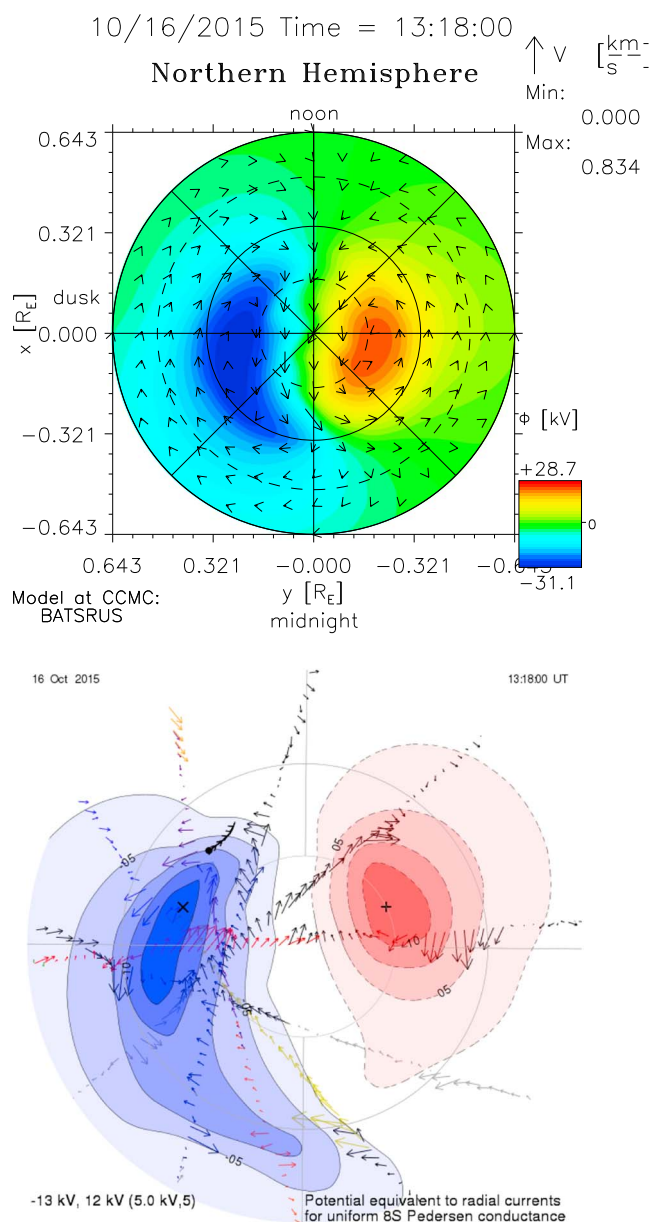


Figure 10. (top) Result from global magnetospheric resistive-MHD simulation showing the polar cap potential in the Northern Hemisphere at 13:18, 11 min after the crossing for the 16 October 2015 event. The arrows denote ionospheric velocity. The total cross polar cap potential is 59.8 kV. (bottom) Polar cap potential for the 16 October 2015 event at 13:18 derived from AMPERE observations. The total cross polar cap potential is 25 kV.

is approximately 0.9 mV/m. This rate is within a factor of 6 of the 2-D PIC simulations and theory, even though the global MHD simulation uses an unrealistic explicit uniform resistivity to break the frozen-in condition.

On the observational side, the cross polar cap potential and the reconnection electric field at the MMS crossing can be inferred from AMPERE (Anderson et al., 2016). The ionospheric convection pattern is derived from the AMPERE field-aligned currents by applying the Ohm's law as described by Merkin and Lyon (2010). In general, ionospheric potential is solved for with a conductance model that incorporates spatially distributed Pedersen and Hall components, which include the solar irradiance and magnetospheric particle precipitation contributions. For the potential inversions presented here, a uniform Pedersen conductance of 8 S is used. The low-latitude boundary condition for the resulting Poisson equation is set to $\Phi = 0$ at 45° magnetic colatitude. We carry out this procedure for the three events considered here. An example is shown for the 16 October 2015 event at 13:18, 11 min after the MMS crossing in Figure 10 (bottom). The results reveal qualitative agreement with the MHD simulations in the top panel. The cross polar cap potential Φ_{CPCP} using this technique is estimated to be 15–29, 18–73, and 8–20 kV for the 16 October 2015, 8 December 2015, and 8 September 2015 events, respectively. The ranges reflect the dependence on the ionospheric conductance model. Using a model magnetosphere to map from the ionosphere to the site of the MMS crossing, the maximum reconnection rate at the site of the crossing is inferred to be 0.2–0.5, 0.29–1.19, and 0.52–1.29 mV/m for the three events. Despite the significant uncertainties with interpreting the AMPERE and resistive-MHD simulations, these rates are within a factor of 2 in all cases to the simulation results and theoretical predictions.

Now, we compare these results with direct observations of out-of-plane electric fields E_{obs} measured by MMS for these events. For the three events, spikes of approximately 15, 100, and 6 mV/m were observed. As has been pointed out previously (Ergun et al., 2016; Eriksson, Wilder, et al., 2016), the observed electric fields are far larger than the predictions, and we confirm here that they are much larger than the local PIC simulations and a global MHD simulation as well—by 1.5 to 3 orders of magnitude. Interestingly, they are also much larger than those inferred from AMPERE observations and the MHD simulations, by a far greater amount than the uncertainty in these results. This is suggestive that the spikes in the MMS data do not correspond to the reconnection electric field in the 2-D steady state sense, as will be discussed further in the next section.

We do point out recent work by Chen et al. (2017) on a different event with a guide field of about 1 (relative to the magnetosheath field; 0.2 relative to the magnetospheric field) from 2015 Dec 14. They filtered the high-frequency signal out of E_M and reported a relatively steady E_M of about 0.84 mV/m which compared well (within a factor of 2) of the rate

obtained from a 2-D PIC simulation. They also saw spikes to higher values that they attributed to double layers. Their result is an example of an event where the maximum rate is also larger than the predicted rate, but they were able to detect a nonzero steady rate in reasonable agreement with simulations that are of the same order of magnitude as the reconnection electric fields inferred here.

There is another way to see if the reconnection process as measured by MMS is revealing signatures of the lower global reconnection rates or the higher local electric fields spikes—the velocity of the reconnection site as it passes by the MMS spacecraft. We focus only on the well-studied 16 October 2015 event. In a steady state, the X line convects into the high magnetic field (magnetospheric) side because it is energetically favorable for the X line to convect than it is to bend the stronger magnetospheric field (Cassak & Shay, 2007).

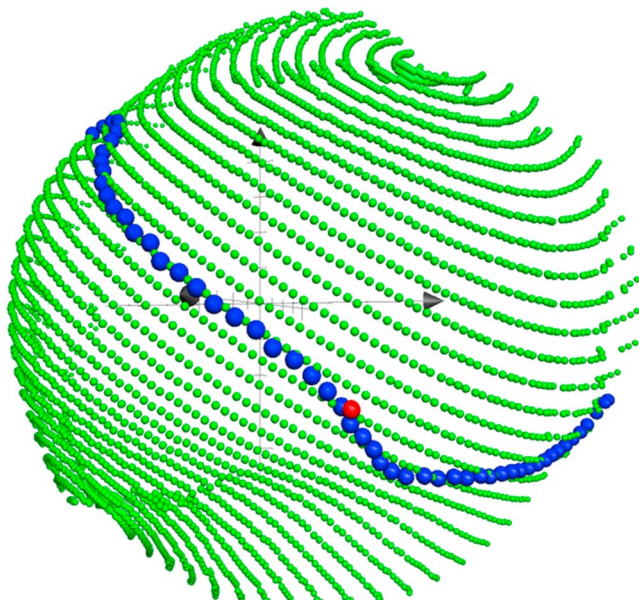


Figure 11. Result from global magnetospheric resistive-MHD simulation of the 16 October 2015 MMS reconnection event showing green dots on the surface of the dayside magnetopause and blue dots for the X line (technically the magnetic separator). The red dot shows the location of the real MMS satellites at the time in the simulation of the real event.

An estimate for the speed it convects earthward assumes that the X line moves at the full inflow velocity. Using the theoretical prediction of $E = 0.70$ mV/m and $B_{L,ms} = 39$ nT for this event, we get an earthward velocity of $E/B_{L,ms} = 18$ km/s. The inferred N directed speed of the structure past the spacecraft is 30–45 km/s (Burch, Torbert, et al., 2016; Ergun et al., 2016). The reasonable agreement between these two is another suggestion that the global dynamics is set by the smaller reconnection electric field rather than the large spikes in E_M observed by MMS. The X line also had a vertical L motion by the spacecraft in the range of 100–200 km/s in the $-L$ direction. We compare this to a superposition of two effects that cause motion of the X line in the L direction. First, we estimate the diamagnetic drift speed to be about 45 km/s in the $+L$ direction. Second, it was suggested that the bulk flow of the magnetosheath can cause an isolated X line to convect (Doss et al., 2015), and under typical conditions the X line speed is comparable to the flow speed. The upstream bulk flow in the magnetosheath is approximately 150 km/s in the $-L$ direction (Burch, Torbert, et al., 2016). A simple superposition of the two speeds gives about 100 km/s in the $-L$ direction. Therefore, the predictions of the speed of the X line both in the N and L directions are reasonably consistent with the observations.

Unsurprisingly, comparing the magnitudes of the measured $\mathbf{J} \cdot \mathbf{E}'$ for the three events in question reveal similarly large disparities between the simulated and measured values, which was anticipated in Eriksson, Wilder, et al. (2016). The simulated peak values are 3.6, 1.1, and 1.1 nW/m³, while the observed peak values are 15, 10, and 8 nW/m³, which differ by up to an order of magnitude.

We now turn to where the energy conversion rate $\mathbf{J} \cdot \mathbf{E}'$ is nonzero and how that depends on guide field. As pointed out in Genestreti et al. (2017), the spikes in $\mathbf{J} \cdot \mathbf{E}'$ are located in different locations relative to the field reversal (X line) on the magnetospheric side. For the low guide field (16 October 2015) event, the spike is displaced from the field reversal (X line) on the magnetospheric side. For the medium guide field (8 December 2015) event, there were two spikes; one at the field reversal (X line) and one near the peak in the current (near the electron stagnation point). For the large guide field (8 September 2015) event, it was very close to the field reversal (X line).

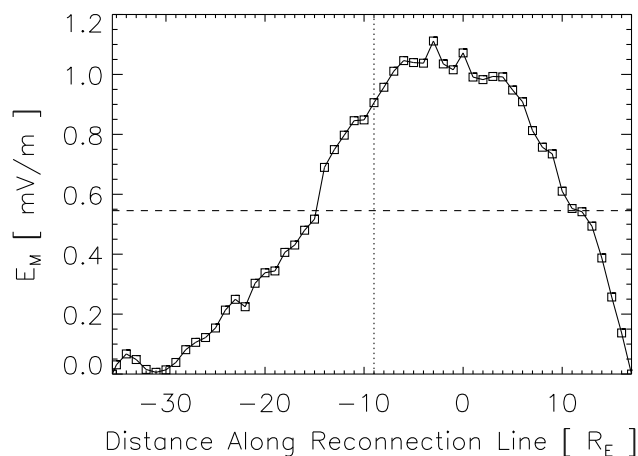


Figure 12. Result from global magnetospheric resistive-MHD simulation of the 16 October 2015 event showing the component of the electric field E in mV/m along the X line (separator) as a function of distance along the X line in Earth radii R_E at the time of the MMS crossing. The zero of the horizontal axis is the subsolar point, and the vertical line at about $-9 R_E$ denotes the location of closest approach of the MMS satellite.

The present results provide some insight into these observations. For the 16 October 2015 event, the predicted location of the electron and ion stagnation points is on the magnetospheric side of the X line. We expect $\mathbf{J} \cdot \mathbf{E}'$ to be peaked halfway between the X line and the electron stagnation point, so it being displaced from the field reversal is qualitatively consistent. Also, using equations (1)–(4) and the upstream parameters in Table 1, the theory predicts $\delta_{XSe} \approx 2$ km. The measured separation between the field reversal and the signal of current density J_M is about 0.3 s, so using an N -directed velocity of 30–45 km/s gives a separation of 9–13.5 km. The prediction is smaller than the inferred size, but the theory also underpredicted the distance in the simulation by a factor of 3, suggesting reasonable agreement between the simulations and observations. That said, it is known that 3-D effects play a role for this event (Ergun et al., 2017; Price et al., 2016) which would be expected to broaden the layer to be thicker than the 2-D theory would predict. Therefore, underpredicting the measured separation is quite reasonable.

For the 8 December 2015 event, there is structure both at the field reversal and toward the magnetosphere where the electron stagnation point is located. This is reasonable given the theoretical predictions, but we do not see such structure in the PIC simulations in a vertical cut through the X line. Finally, for the 8 September 2015 event, the structure is near the X line.

We expect the structure to be close to the electron stagnation point. However, due to the large guide field, the diffusion region is thinner, so it should be closer to the X line in an absolute sense. This is consistent with the data. Thus, there are some similarities to the data, but there are also important differences that still need to be understood.

Finally, we qualitatively compare distribution functions between the 2-D simulations and the observational data from MMS for these three events. For the low guide field 16 October 2015 event, crescent distribution functions were observed; see Figure 4 of Burch, Torbert, et al. (2016). For the guide field 1 case in Burch and Phan (2016), crescents were also observed, but they were less pronounced. For the strong guide field case in Eriksson, Wilder, et al. (2016), no crescent distribution functions were reported. This is consistent with the predictions by Hesse et al. (2014, 2016), and consistent with the distribution functions seen in the present study as seen in Figures 7–9.

As before, we promote caution in these types of comparisons. Indeed, since it is not likely the spikes in electric field in the data are the same as what is seen in these 2-D simulations, it is not obvious whether any correspondence is meaningful. This warrants further study; 3-D simulations will be an asset for such future work.

6. Summary and Discussion

This study is motivated by observations of three magnetic reconnection events by MMS that revealed the location where the rate of energy conversion by the electric field in the reference frame of the electrons $\mathbf{J} \cdot \mathbf{E}'$ is appreciable depends on the strength of the out-of-plane guide magnetic field. We perform a theoretical and computational study to address this issue. In this study, we argued on theoretical grounds that the peak in the current is expected to lie between the X line and the electron stagnation point for typical conditions at the dayside magnetopause. (Note, one can simulate cases for which this is not the case (Malakit, 2012).) We argue it is between the X line and electron stagnation point in the weak guide field limit, and moves toward the electron stagnation point with increasing guide field (for typical magnetospheric conditions). Physically, the current is carried by electrons making up the crescent-shaped distribution in the weak guide field case. As the guide field increases and more electrons remain magnetized by the guide field, the out-of-plane current is carried by particles accelerating along the guide field by the reconnection electric field.

We suggest a nonrigorous approach to generalize previous predictions for the location of the X line and stagnation points to the case with a guide field. We then compare the predictions to results of 2-D PIC simulations using upstream parameters guided by the MMS observations of three events. We find the new predictions do a reasonable job of capturing the scaling of the changes with the guide field. The dominant effect of the guide field controlling the distance between the X line and where the energy conversion occurs is the gyroradius of the electrons, which decreases with increasing guide field. A number of effects were not included and could affect the scaling, including diamagnetic effects, 3-D effects, and effects due to time variation, which should be addressed in future work.

The results imply the following about the relative and absolute location of where the energy conversion rate is a maximum. In the relative sense, the energy conversion moves from midway between the X line and electron stagnation point for the zero guide field case to close to the electron stagnation point for the strong guide field case. In the absolute sense, the thickness of the diffusion region decreases with increasing guide field, so the energy conversion appears closer to the X line compared to weaker guide field events.

We also confirmed the previously noted result that the strong spikes in out-of-plane electric field observed in a number of MMS reconnection events far exceed the reconnection rate predicted from 2-D steady state reconnection theory (Ergun et al., 2016; Eriksson, Wilder, et al., 2016). There seems to be broad agreement that the measured electric fields cannot be representing the uniform reconnection electric field envisioned in 2-D reconnection theory. Indeed, if the high values observed represented the reconnection electric field, then the cross polar cap potential would be far greater than what is observed, as shown here using AMPERE observations and global magnetospheric simulations, so these strong fields cannot be global.

There is less certainty on what the strong out-of-plane electric fields seen by MMS do represent. It has been suggested that they represent the electric field that arises due to drift waves, where the rippling of the density gradient causes the normal electric field to rotate into the M direction. Stronger electric fields than those measured in the 2-D simulations presented here have been found, for the 16 October 2015 event, in 3-D

simulations using the same upstream parameters (Le et al., 2017; Price et al., 2016; 2017), suggesting that 3-D simulations are crucial to satisfactorily address this issue. It has also been suggested that these fields truly represent reconnection which is bursty and localized and the average over the bursty fields gives the global rate in agreement with global considerations, but this remains an open question. We do, however, point out that some of the MMS events, including the 16 October 2015 and 8 September 2015 events have unipolar spikes in the out-of-plane electric field, while others like the 8 December 2015 event have strong electric field signatures with bipolar spikes.

Since the large spikes in out-of-plane electric field in the MMS data do not correspond to the uniform reconnection electric field in the simulations, we refrain from making too strong of a statement about whether the simulations agree with the observations on the location of the regions where $\mathbf{J} \cdot \mathbf{E}'$ is nonzero but a number of aspects do agree with the theory and simulations. In future work, it will be interesting to revisit the questions here in 3-D simulations, both for the larger-scale reconnection electric field and the structured spikes that arise. The fully 3-D system is, of course, more complicated. Without a guide field, 3-D features such as electron holes, the Buneman instability, and electrostatic whistlers can trap particles in the wave fields leading to irreversible dissipation (Che et al., 2011; Drake et al., 2003). Similarly, with a guide field, drift waves are associated with strong electric fields which may or may not be dissipative. Both reversible energy conversion and irreversible dissipation is included in $\mathbf{J} \cdot \mathbf{E}'$. It has been, and remains, a challenge to determine how a signal of nonzero $\mathbf{J} \cdot \mathbf{E}'$ is partitioned between reversible and irreversible energy conversion.

Acknowledgments

We gratefully acknowledge support from the following sources: P.A.C.: NASA grants NNX16AF75G and NNX16AG76G; M. A. S.: NNX15AW58G and NNX08A083G-MMS IDS; C. M. K.: the NASA Living With a Star Program as part of the Targeted Science Team on Radiation Belt Response to Interplanetary Structures; and S. E.: NASA MMS-Phase E support to CU/LASP and NASA grant NNX08AO84G. P. A. C. appreciates the efforts of all the MMS team members for their hard work in making a successful mission. This research uses resources of the National Energy Research Scientific Computing Center (NERSC), a DOE Office of Science User Facility supported by the Office of Science of the U.S. Department of Energy under contract DE-AC02-05CH11231. PIC simulation data are archived at NERSC and can be made available from the corresponding author by request. Global simulations were performed at the Community Coordinated Modeling Center (CCMC) at Goddard Space Flight Center through their public Runs on Request system (<http://ccmc.gsfc.nasa.gov>). The CCMC is a multiagency partnership between NASA, AFMC, AFOSR, AFRL, AFWA, NOAA, NSF, and ONR. The BATS-R-US model was developed by the Center for Space Environment Modeling at the University of Michigan. The global simulation analysis presented here was made possible via the Kameleon software package provided by the CCMC. Software Developers are as follows: M. M. Maddox, D. H. Berrios, and L. Rastaetter. The global simulation data used to produce the results of this paper are publicly available for free at the CCMC; the run name is Colin_Komar_042616_2.

References

- Anderson, B. J., Russell, C. T., Strangeway, R. J., Plaschke, F., Magnes, W., ... Burch, J. L. (2016). Electrodynamic context of magnetopause dynamics observed by magnetospheric multiscale. *Geophysical Research Letters*, *43*, 5988–5996. <https://doi.org/10.1002/2016GL069577>
- Angelopoulos, V., Runov, A., Zhou, X.-Z., Turner, D. L., Kiehas, S. A., Li, S.-S., & Shinohara, I. (2013). Electromagnetic energy conversion at reconnection fronts. *Science*, *341*, 1478–1482.
- Beidler, M. T., & Cassak, P. A. (2011). Model for incomplete reconnection in sawtooth crashes. *Physical Review Letters*, *107*, 255002.
- Bessho, N., Chen, L.-J., & Hesse, M. (2016). Electron distribution functions in the diffusion region of asymmetric magnetic reconnection. *Geophysical Research Letters*, *43*, 1828–1836. <https://doi.org/10.1002/2016GL067886>
- Birdsall, C. K., & Langdon, A. B. (2004). *Plasma physics via computer simulation*. London: Taylor & Francis.
- Burch, J. L., & Phan, T. D. (2016). Magnetic reconnection at the dayside magnetopause: Advances with MMS. *Geophysical Research Letters*, *43*, 8327–8338. <https://doi.org/10.1002/2016GL069787>
- Burch, J. L., Moore, T. E., Torbert, R. B., & Giles, B. L. (2016). Magnetospheric multiscale overview and science objectives. *Space Science Reviews*, *199*, 5–21.
- Burch, J. L., Torbert, R. B., Phan, T. D., Chen, L.-J., Moore, T. E., Ergun, R. E., ... Chandler, M. (2016). Electron-scale measurements of magnetic reconnection in space. *Science*, *352*(6290), aaf2939.
- Cassak, P. A., & Shay, M. A. (2007). Scaling of asymmetric magnetic reconnection: General theory and collisional simulations. *Physics of Plasmas*, *14*, 102114. <https://doi.org/10.1029/2008GL035268>
- Cassak, P. A., & Shay, M. A. (2008). Scaling of asymmetric Hall reconnection. *Geophysical Research Letters*, *35*, L19102. <https://doi.org/10.1029/2008GL035268>
- Cassak, P. A., & Shay, M. A. (2009). Structure of the dissipation region in fluid simulations of asymmetric magnetic reconnection. *Physics of Plasmas*, *16*, 055704.
- Che, H., Drake, J. F., & Swisdak, M. (2011). A current filamentation mechanism for breaking magnetic field lines during reconnection. *Nature*, *474*, 184–187. <https://doi.org/10.1038/nature10091>
- Chen, L.-J., Hesse, M., Wang, S., Gershman, D., Ergun, R. E., Burch, J., ... Avano, L. (2017). Electron diffusion region during magnetopause reconnection with an intermediate guide field: Magnetospheric multiscale observations. *Journal of Geophysical Research*, *122*, 5235–5246. <https://doi.org/10.1002/2017JA024004>
- Coppi, B. (1965). Current-driven instabilities in configurations with sheared magnetic fields. *Physics of Fluids*, *8*, 2273–2280.
- Daughton, W. (2013). Electromagnetic properties of the lower-hybrid drift instability in a thin current sheet. *Physics of Plasmas*, *10*, 3103–3119.
- Davidson, R. C., & Gladd, N. T. (1975). Anomalous transport properties associated with the lower-hybrid-drift instability. *Physics of Fluids*, *18*, 1327–1335.
- De Zeeuw, D. L., Gombosi, T. I., Groth, C. P. T., Powell, K. G., & Scott, Q. F. (2000). An adaptive MHD method for global space weather simulations. *IEEE Transactions on Plasma Science*, *28*, 1956–1965.
- DiBaccio, G. A., Slavin, J. A., Boardsen, S. A., Anderson, B. J., Korth, H., & Zurbuchen, T. H. (2013). MESSENGER observations of magnetopause structure and dynamics at Mercury. *Journal of Geophysical Research: Space Physics*, *118*, 997–1008. <https://doi.org/10.1002/jgra.50123>
- Doss, C. E., Komar, C. M., Cassak, P. A., Wilder, F. D., Eriksson, S., & Drake, J. F. (2015). Asymmetric magnetic reconnection with a flow shear and applications to the magnetopause. *Journal of Geophysical Research: Space Physics*, *120*, 7748–7763. <https://doi.org/10.1002/2015JA021489>
- Doss, C. E., Cassak, P. A., & Swisdak, M. (2016). Particle-in-cell simulation study of the scaling of asymmetric magnetic reconnection with in-plane flow shear. *Physics of Plasmas*, *23*, 082107.
- Drake, J. F., Swisdak, M., Che, H., & Shay, M. A. (2006). Electron acceleration from contracting magnetic fields during reconnection. *Nature*, *443*, 553–556.
- Drake, J. F., Swisdak, M., Shay, M. A., Rogers, B. N., Zeiler, A., & Cattell, C. (2003). Formation of electron holes and particle energization during magnetic reconnection. *Science*, *299*, 873–877.
- Dungey, J. W. (1953). Conditions for the occurrence of electrical discharges in astrophysical systems. *Philosophical Magazine*, *44*, 725–738.
- Dungey, J. W. (1961). Interplanetary magnetic field and the auroral zones. *Physical Review Letters*, *6*, 47.

- Egedal, J., Daughton, W., Le, A., & Borg, A. L. (2015). Double layer electric fields aiding the production of energetic flat-top distributions and superthermal electrons within magnetic reconnection exhausts. *Physics of Plasmas*, 22, 101208.
- Ek-In, S., Malakit, K., Ruffolo, D., Shay, M. A., & Cassak, P. A. (2017). Effects of a guide field on the Larmor electric field and upstream electron temperature anisotropy in collisionless asymmetric reconnection. *The Astrophysical Journal*, 845, 113.
- Ergun, R. E., Chen, L.-J., Wilder, F. D., Ahmadi, N., Eriksson, S., Usanova, M. E., ... Nakamura, R. (2017). Drift waves, intense parallel electric fields, and turbulence associated with asymmetric magnetic reconnection at the magnetopause. *Geophysical Research Letters*, 44, 2978–2986. <https://doi.org/10.1002/2016GL072493>
- Ergun, R. E., Goodrich, K. A., Wilder, F. D., Holmes, J. C., Stawarz, J. E., Eriksson, S., ... Marklund, G. (2016). Magnetospheric multiscale satellites observations of parallel electric fields associated with magnetic reconnection. *Physical Review Letters*, 116, 235102.
- Eriksson, S., Lavraud, B., Wilder, F. D., Stawarz, J. E., Giles, B. L., Burch, J. L., ... Goodrich, K. A. (2016). Magnetospheric multiscale observations of magnetic reconnection associated with Kelvin-Helmholtz waves. *Geophysical Research Letters*, 43, 5606–5615. <https://doi.org/10.1002/2016GL068783>
- Eriksson, S., Wilder, F. D., Ergun, R. E., Schwartz, S. J., Cassak, P. A., Burch, J. L., ... Marklund, G. T. (2016). Magnetospheric multiscale observations of the electron diffusion region of large guide field magnetic reconnection. *Physical Review Letters*, 117, 015001.
- Fu, H. S., Vaivads, A., Khotyaintsev, Y. V., André, M., Cao, J. B., Olshevsky, V., ... Retinò, A. (2017). Intermittent energy dissipation by turbulent reconnection. *Geophysical Research Letters*, 44, 37–43. <https://doi.org/10.1002/2016GL071787>
- Fuselier, S. A., Frahm, R., Lewis, W. S., Masters, A., Mukherjee, J., Petrinec, S. M., & Sillanpaa, I. J. (2014). The location of magnetic reconnection at Saturn's magnetopause—A comparison with Earth. *Journal of Geophysical Research: Space Physics*, 119, 2563–2578. <https://doi.org/10.1002/2013JA019684>
- Fuselier, S. A., Vines, S. K., Burch, J. L., Petrinec, S. M., Trattner, K. J., Cassak, P. A., ... Webster, J. M. (2017). Large-scale characteristics of reconnection diffusion regions and associated magnetopause crossings observed by MMS. *Journal of Geophysical Research: Space Physics*, 122, 5466–5486. <https://doi.org/10.1002/2017JA024024>
- Genestreti, K. J., Burch, J. L., Cassak, P. A., Torbert, R. B., Ergun, R. E., Phan, T. D., ... Varsani, A. (2017). The effect of a guide field on local energy conversion during asymmetric magnetic reconnection: MMS observations. *Journal of Geophysical Research*, 122. <https://doi.org/10.1002/2017JA024247>
- Gombosi, T., De Zeeuw, D., Groth, C., & Powell, K. (2000). Magnetospheric configuration for Parker-spiral IMF conditions: Results of a 3D AMR MHD simulation. *Advances in Space Research*, 26, 139–149.
- Guzdar, P. N., Drake, J. F., McCarthy, D., Hassam, A. B., & Liu, C. S. (1993). Three-dimensional fluid simulations of the nonlinear drift-resistive ballooning modes in tokamak edge plasmas. *Physics of Fluids B*, 5(10), 3712–3727.
- Haggerty, C. C., Shay, M. A., Phan, T. D., & McHugh, C. T. (2015). The competition of electron and ion heating during magnetic reconnection. *Geophysical Research Letters*, 42, 9657–9665. <https://doi.org/10.1002/2015GL065961>
- Hesse, M., Aunai, N., Sibeck, D., & Birn, J. (2014). On the electron diffusion region in planar, asymmetric, systems. *Geophysical Research Letters*, 41, 8673–8680. <https://doi.org/10.1002/2014GL061586>
- Hesse, M., Liu, Y.-H., Chen, L.-J., Bessho, N., Kuznetsova, M., Birn, J., & Burch, J. L. (2016). On the electron diffusion region in asymmetric reconnection with a guide magnetic field. *Geophysical Research Letters*, 43, 2359–2364. <https://doi.org/10.1002/2016GL068373>
- Hietala, H., Artemyev, A. V., & Angelopoulos, V. (2017). Ion dynamics in magnetotail reconnection in the presence of density asymmetry. *Journal of Geophysical Research: Space Physics*, 122, 2010–2023. <https://doi.org/10.1002/2016JA023651>
- Huba, J. D., Gladd, N. T., & Papadopoulos, K. (1977). The lower-hybrid-drift instability as a source of anomalous resistivity for magnetic field reconnection. *Geophysical Research Letters*, 4, 125.
- Komar, C. M., & Cassak, P. A. (2016). The local dayside reconnection rate for oblique interplanetary magnetic fields. *Journal of Geophysical Research*, 121, 5105–5120. <https://doi.org/10.1002/2016JA022530>
- Komar, C. M., Cassak, P. A., Dorelli, J. C., Gloer, A., & Kuznetsova, M. M. (2013). Tracing magnetic separators and their dependence on IMF clock angle in global magnetospheric simulations. *Journal of Geophysical Research: Space Physics*, 118, 4998–5007. <https://doi.org/10.1002/jgra.50479>
- Le, A., Daughton, W., Chen, L.-J., & Egedal, J. (2017). Enhanced electron mixing and heating in 3-D asymmetric reconnection at the Earth's magnetopause. *Geophysical Research Letters*, 44, 2096–2104. <https://doi.org/10.1002/2017GL072522>
- Levy, R. H., Petschek, H. E., & Siscoe, G. L. (1964). Aerodynamic aspects of magnetospheric flow. *AIAA Journal*, 2, 2065–2076.
- Liu, Y.-H., Hesse, M., Guo, F., Daughton, W., Li, H., Cassak, P. A., & Shay, M. A. (2017). Why does steady-state magnetic reconnection have a maximum local rate of order 0.1? *Physical Review Letters*, 118, 085101.
- Malakit, K. (2012). Asymmetric magnetic reconnection: A particle-in-cell study (PhD thesis), USA.
- Malakit, K., Shay, M. A., Cassak, P. A., & Bard, C. (2010). Scaling of asymmetric magnetic reconnection: Kinetic particle-in-cell simulations. *Journal of Geophysical Research*, 115, A10223. <https://doi.org/10.1029/2010JA015452>
- Masters, A., Eastwood, J. P., Swisdak, M., Thomsen, M. F., Russell, C. T., Sergis, N., ... Krimigis, S. M. (2012). The importance of plasma β conditions for magnetic reconnection at Saturn's magnetopause. *Geophysical Research Letters*, 39, L08103. <https://doi.org/10.1029/2012GL051372>
- McPherron, R. L., Russell, C. T., & Aubry, M. P. (1973). Phenomenological model for substorms. *Journal of Geophysical Research*, 78, 3131–3149.
- Merkin, V. G., & Lyon, J. G. (2010). Effects of the low-latitude ionospheric boundary condition on the global magnetosphere. *Journal of Geophysical Research*, 115, A10202. <https://doi.org/10.1029/2010JA015461>
- Mozer, F., Bale, S. D., & Phan, T. D. (2002). Evidence of diffusion regions in a subsolar magnetopause crossing. *Physical Review Letters*, 89, 015002.
- Murphy, N. A., Miralles, M. P., Pope, C. L., Raymond, J. C., Winter, H. D., Reeves, K. K., ... Lin, J. (2012). Asymmetric magnetic reconnection in solar flare and coronal mass ejection current sheets. *The Astrophysical Journal*, 751, 56.
- Nykyri, K., & Otto, A. (2001). Plasma transport at the magnetospheric boundary due to reconnection in Kelvin-Helmholtz vortices. *Geophysical Research Letters*, 28, 3565–3568.
- Øieroset, M., Phan, T. D., & Fujimoto, M. (2004). Wind observations of asymmetric magnetic reconnection in the distant magnetotail. *Geophysical Research Letters*, 31, L12801. <https://doi.org/10.1029/2004GL019958>
- Powell, K. G., Roe, P. L., Linde, T. J., Gombosi, T. I., & De Zeeuw, D. L. (1999). A solution-adaptive upwind scheme for ideal magnetohydrodynamics. *Journal of Computational Physics*, 154, 284–309.
- Price, L., Swisdak, M., Drake, J. F., Cassak, P. A., Dahlin, J. T., & Ergun, R. E. (2016). The effects of turbulence on three-dimensional magnetic reconnection at the magnetopause. *Geophysical Research Letters*, 43, 6020–6027. <https://doi.org/10.1002/2016GL069578>
- Price, L., Swisdak, M., Drake, J. F., Burch, J. L., Cassak, P. A., & Ergun, R. E. (2017). Turbulence associated with magnetopause reconnection. *Journal of Geophysical Research*, 122. <https://doi.org/10.1002/2017JA024227>

- Pritchett, P. L. (2006). Relativistic electron production during guide field magnetic reconnection. *Journal of Geophysical Research*, *111*, A10212. <https://doi.org/10.1029/2006JA011793>
- Pritchett, P. L. (2008). Collisionless magnetic reconnection in an asymmetric current sheet. *Journal of Geophysical Research*, *113*, A06210. <https://doi.org/10.1029/2007JA012930>
- Rogers, B., & Zakharov, L. (1995). Nonlinear ω_s stabilization of the $m = 1$ mode in tokamaks. *Physics of Plasmas*, *2*, 3420–3428.
- Rogers, B. N., Kobayashi, S., Ricci, P., Dorland, W., Drake, J., & Tatsuno, T. (2007). Gyrokinetic simulations of collisionless magnetic reconnection. *Physics of Plasmas*, *14*, 092110.
- Roytershteyn, V., Daughton, W., Karimabadi, H., & Mozer, F. S. (2012). Influence of the lower-hybrid drift instability on magnetic reconnection in asymmetric configuration. *Physical Review Letters*, *108*, 185001.
- Servidio, S., Matthaeus, W. H., Shay, M. A., Cassak, P. A., & Dmitruk, P. (2009). Magnetic reconnection in two-dimensional magnetohydrodynamic turbulence. *Physical Review Letters*, *102*, 115003.
- Servidio, S., Matthaeus, W. H., Shay, M. A., Dmitruk, P., Cassak, P. A., & Wan, M. (2010). Statistics of magnetic reconnection in two-dimensional magnetohydrodynamic turbulence. *Physical Review Letters*, *17*, 032315.
- Shay, M. A., Drake, J. F., Rogers, B. N., & Denton, R. E. (1999). The scaling of collisionless, magnetic reconnection for large systems. *Geophysical Research Letters*, *26*, 2163–2166.
- Shay, M. A., Haggerty, C. C., Phan, T. D., Drake, J. F., Cassak, P. A., Wu, P., ... Malakit, K. (2014). Electron heating during magnetic reconnection: A simulation scaling study. *Physics of Plasmas*, *21*, 122902.
- Shay, M. A., Phan, T. D., Haggerty, C. C., Fujimoto, M., Drake, J. F., Malakit, K., ... Swisdak, M. (2016). Kinetic signatures of the region surrounding the X-line in asymmetric (magnetopause) reconnection. *Geophysical Research Letters*, *43*, 4145–4154. <https://doi.org/10.1002/2016GL069034>
- Swisdak, M., Drake, J. F., Shay, M. A., & Rogers, B. N. (2003). Diamagnetic suppression of component magnetic reconnection at the magnetopause. *Journal of Geophysical Research*, *108*, 1218. <https://doi.org/10.1029/2002JA009726>
- Swisdak, M., Drake, J. F., Shay, M. A., & McIlhargey, J. G. (2005). The transition from antiparallel to component magnetic reconnection. *Journal of Geophysical Research*, *110*, A05210. <https://doi.org/10.1029/2004JA010748>
- Swisdak, M., Opher, M., Drake, J. F., & Alouani Bibi, F. (2010). The vector direction of the interstellar magnetic field outside the heliosphere. *The Astrophysical Journal*, *710*(2), 1769–1775. <https://doi.org/10.1088/0004-637X/710/2/1769>
- Vasyliunas, V. M. (1975). Theoretical models of magnetic field line merging, 1. *Reviews of Geophysics*, *13*(1), 303–336.
- Walsh, B. M., Phan, T. D., Sibeck, D. G., & Souza, V. M. (2014). The plasmaspheric plume and magnetopause reconnection. *Geophysical Research Letters*, *41*, 223–228. <https://doi.org/10.1002/2013GL058802>
- Yoo, Y., Yamada, M., Ji, H., Jara-Almonte, J., Myers, C. E., & Chen, L.-J. (2014). Laboratory study of magnetic reconnection with a density asymmetry across the current sheet. *Physical Review Letters*, *113*, 095002.
- Zakharov, L., & Rogers, B. (1992). Two-fluid magnetohydrodynamic description of the internal kink mode in tokamaks. *Physics of Fluids B*, *4*, 3285–3301.
- Zeiler, A., Biskamp, D., Drake, J. F., Rogers, B. N., Shay, M. A., & Scholer, M. (2002). Three-dimensional particle simulations of collisionless magnetic reconnection. *Journal of Geophysical Research*, *107*, 1230. <https://doi.org/10.1029/2001JA000287>
- Zenitani, S., Hesse, M., Klimas, A., & Kuznetsova, M. (2011). New measure of the dissipation region in collisionless magnetic reconnection. *Physical Review Letters*, *106*, 195003.
- Zweibel, E. G., & Yamada, M. (2009). Magnetic reconnection in astrophysical and laboratory plasmas. *Annual Review of Astronomy and Astrophysics*, *47*, 291–332.